Analyzing the Role of Fragment Charge on Nuclear Stopping for Symmetric Colliding Nuclei

Dissertation submitted in the partial fulfilment of the requirement for

The award of the degree of

Master of Science
in
Physics

Submitted by

T. Sahil

Roll No- 301104017

Under the guidance of

Dr. Suneel Kumar

School Of Physics and Materials Science

Thapar University

Patiala – 147004 (PUNJAB)

INDIA

CERTIFICATE

I hereby declare that the report entitled "**Analyzing the Role of Fragment Charge on Nuclear Stopping for Symmetric Colliding Nuclei**" is an authentic record of my own work carried out for the partial fulfilment of the requirement for the award of the degree of M.Sc. (Masters of Science) at Thapar University, Patiala (Punjab), under the guidance of Dr. Suneel Kumar (School of Physics and Materials Science). The matter presented in the dissertation has not been submitted in part or full for the award of any other degree.

Date: 11/6/2013

T. Sahil

Roll No. : 301104017

It is certified that the above statement made by the candidate is correct to the best of my knowledge and belief.

SKumar 11/6/2013

(Dr. Suneel Kumar)

Associate Professor

School of Physics and Materials Science

Thapar University, Patiala

26/6/13

(Dr. Kulvir Singh)

(Head)

School of Physics and Materials Science

Thapar University, Patiala

(Dr. S.K. Mohapatra)

Dean of Academic Affairs

Thapar University, Patiala

ACKNOWLEDGEMENTS

Foremost, I would like to express my sincere gratitude to my supervisor **Dr. Suneel Kumar** for his continuous support and supervision, for his patience, motivation, enthusiasm, and immense knowledge. His guidance helped me at all times of research and in writing of this dissertation. I could not have imagined having a better advisor and mentor for my thesis.

I would like to thank **Dr. Kulvir Singh**, Head, School of Physics and Materials Science for his support and providing me the necessary lab facilities.

I express my deepest gratitude to **Miss Anupriya Jain**, without whom I would not have been able to complete my dissertation. My sincere thanks to the research scholars of the physics department for their help and valuable suggestions.

I also acknowledge my friends at School of Physics and Materials Science, for their insightful views and ideas.

I am deeply thankful to my family, for their moral support and patience which gave me the necessary motivation and strength to endure research and complete my thesis.

Date: 11/6/2013

T.Sahil

Place: Thapar University, Patiala

Roll No. 301104017

ABSTRACT

We study the role of fragment charge as well as the isospin dependence of nucleon-nucleon cross-section on nuclear stopping using isospin dependent quantum molecular dynamics model. The analysis is carried out for the symmetric reactions $^{40}_{20}$Ca +$^{40}_{20}$Ca, $^{58}_{28}$Ni +$^{58}_{28}$Ni, $^{129}_{54}$Xe +$^{129}_{54}$Xe, and $^{197}_{79}$Au +$^{197}_{79}$Au, spanning over the energy range 90 MeV/nucleon – 1.5 GeV/nucleon. For the fragment formation, we use three different clusterization algorithms MST (Minimum Spanning Tree), MSTP (Minimum Spanning Tree with momentum constraint), iso-MST (isospin dependent Minimum Spanning Tree). Stopping parameter *varxz* for protons and different fragment charge is calculated as a function of various parameters, taking into account both isospin dependent and isospin independent cross-section as well as the different clusterization techniques. The theoretical findings are compared with the experimental findings of the FOPI data.

CONTENTS

Chapter 2: Methodology

Chapter 3: Nuclear Stopping in Heavy Ion Collisions

List of Figures Page No.

Chapter 1

INTRODUCTION

1.1 Heavy ion Physics

Nuclear physics has come a long way to provide us a clear picture of the nuclear processes. Many observable and predictable phenomena can be explained and visualized with the help of *Heavy Ion Collisions*.

One of the main interests to study heavy-ion collisions is the investigation of the properties of nuclear matter under extreme conditions of density and temperature [1-8]. These investigations include the production of secondary particles, the properties of particles in a (dense) nuclear medium, the compression and repulsion of dense nuclear matter, its equilibration during the reaction and its decay into fragments and single particles.

Various phenomena occurring in nuclear physics can further be divided into three categories depending on the incident energy of the colliding nuclei. [9];

1.1.1 Low Energy Regime (Energy $\leq$ 10 MeV/nucleon): This energy regime deals with nuclear interactions, fusion-fission, cluster-radioactivity, formation of super heavy elements through the neutron rich radioactive beams, the halo nuclei [10-13], etc. In other words, the nuclear physics at low incident energy focuses mainly on the structure of the nuclei. The reaction cross-section at low incident energies composes of three categories i.e. fusion, quasi-elastic and deep inelastic scattering. At low incident energy, the colliding nuclei cannot compress each other so majority of the collisions are blocked due to lack of available free phase space. At such incident energy, the nucleon-nucleon collisions are negligible and mean field is maximum.

1.1.2 Intermediate Energy Regime (10 MeV/nucleon < Energy $\leq$ 2 GeV/nucleon)**:** In this energy regime, both mean field and nucleon-nucleon collisions play important role. Both these factors together contribute in dissembling the matter from an initial fused state. [14] Due to the formation of compressed and hot piece of nuclear matter at intermediate energies, it gives possibility to study the properties of nuclear matter under extreme conditions. At such energies, heavy ion collisions compress the protons and neutrons to 2-

3 times the normal nuclear matter densities and a typical temperature of 100 MeV can be reached. [15] This branch investigates the behaviour of hadrons, generation of high density matter, heavy ion collisions, Multi-fragmentation, nuclear stopping, collective flow, sub-threshold particle production etc. [9]

1.1.3 High Energy Regime (E > 2 GeV/nucleon)**:** In this regime, the temperature and densities are very high. Due to very high incident energy, there is availability of large phase space which makes the role of Pauli blocking negligible, and therefore roughly 4% collisions are blocked [15]. The dynamics of reactions involved at high energy are chiefly governed by nucleon-nucleon collisions. This branch, aims in studying the fundamental particles and their interactions, and the search for grand unified theory.

The study and investigation of heavy ion collisions (HIC's) and its dynamics becomes important in understanding phenomena such as multifragmentation, collective flow, and nuclear stopping which provide us with essential information about the bulk properties of nuclear matter which are used to understand the phenomena like origin of early universe and supernova explosions etc. In the following subsection, we shall discuss these various phenomena occurring at intermediate energy regime in brief.

1.2 Mutifragmentation

Multifragmentation refers to the process where large number of particles are produced in an energetic heavy-ion reaction shown in Fig.1.1 [14]. The produced particles include the free particles (A = 1), light charged particles ($2 \leq A \leq 4$), Medium mass fragments ($5 \leq A \leq 9$) as well as Intermediate mass fragments ($5 \leq A \leq A_{tot}/6$). The production of these fragments depends on incident energy, impact parameter, colliding geometry and equation of state (EOS). Multifragmentation process can thus be linked with understanding the reaction dynamics and parameters such as the EOS and in medium nucleon-nucleon cross-section. Factors such as momentum dependent interactions (MDI), asymmetry of the reaction are found to affect multifragmentation, which can be better understood by using the more sophisticated models like IQMD [20] in which neutrons and protons can be separated on the basis of charge.

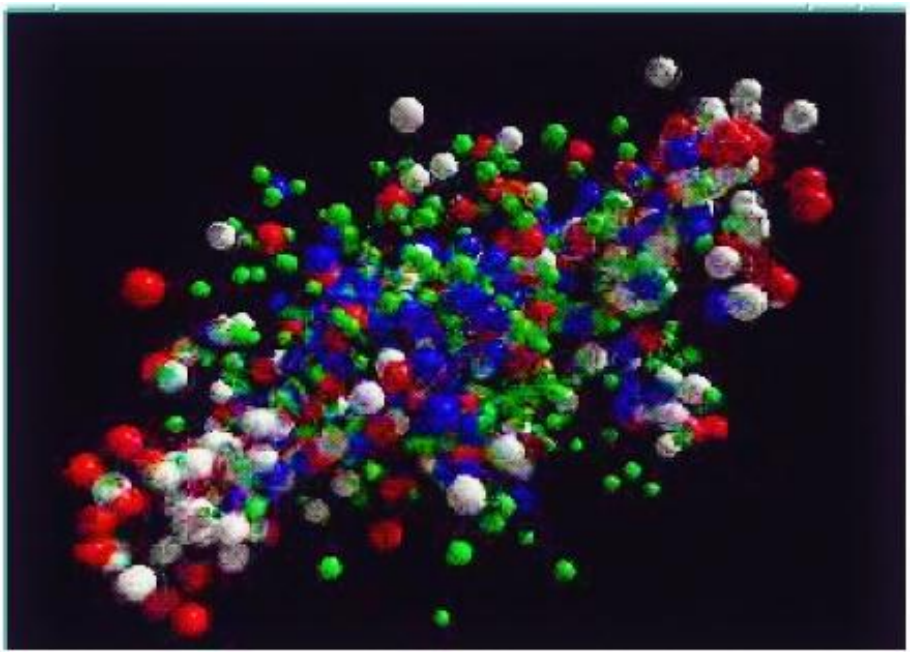

Fig. 1.1: Multifragmentation after a heavy ion collision. The different colours represent various fragments of different energies [14].

1.3 Collective Flow

The Collective flow is a measure of the transverse motion or momentum imparted to particles and fragments during the collision of two nuclei. The evolution of collective flow depends on the pressure build-up during the compression stage after the collision of the two nuclei. It provides us the information about the pressure and particle density relation, that is, the EOS of the system. During the decompression stage, the direction and the speed of the particles is towards the region of the lower pressure. There are three types of flow, namely, radial, directed and elliptical flow. The radial flow arises in central collisions and is characterized by the high kinetic energy spectra of the particles emitted near θc.m. = 90^0 relative to the beam axis. On the other hand, directed flow, also called ”in-plane” or ”side wards” flow, refers to the preferential emission of particles within, and to a particular side of, the reaction plane (reaction plane is defined as the plane which contains the beam axis and a line joining the centres of the two nuclei). In case of directed flow, the ϕ distribution for forward rapidity ($Y_{c.m} > 0$) and backward rapidity ($Y_{c.m} < 0$) is anti-symmetric, whereas elliptical flow has the same distribution in both rapidity regions, at least for symmetric reactions. The elliptical flow indicates whether the particle emission is in-plane or out-of-plane.

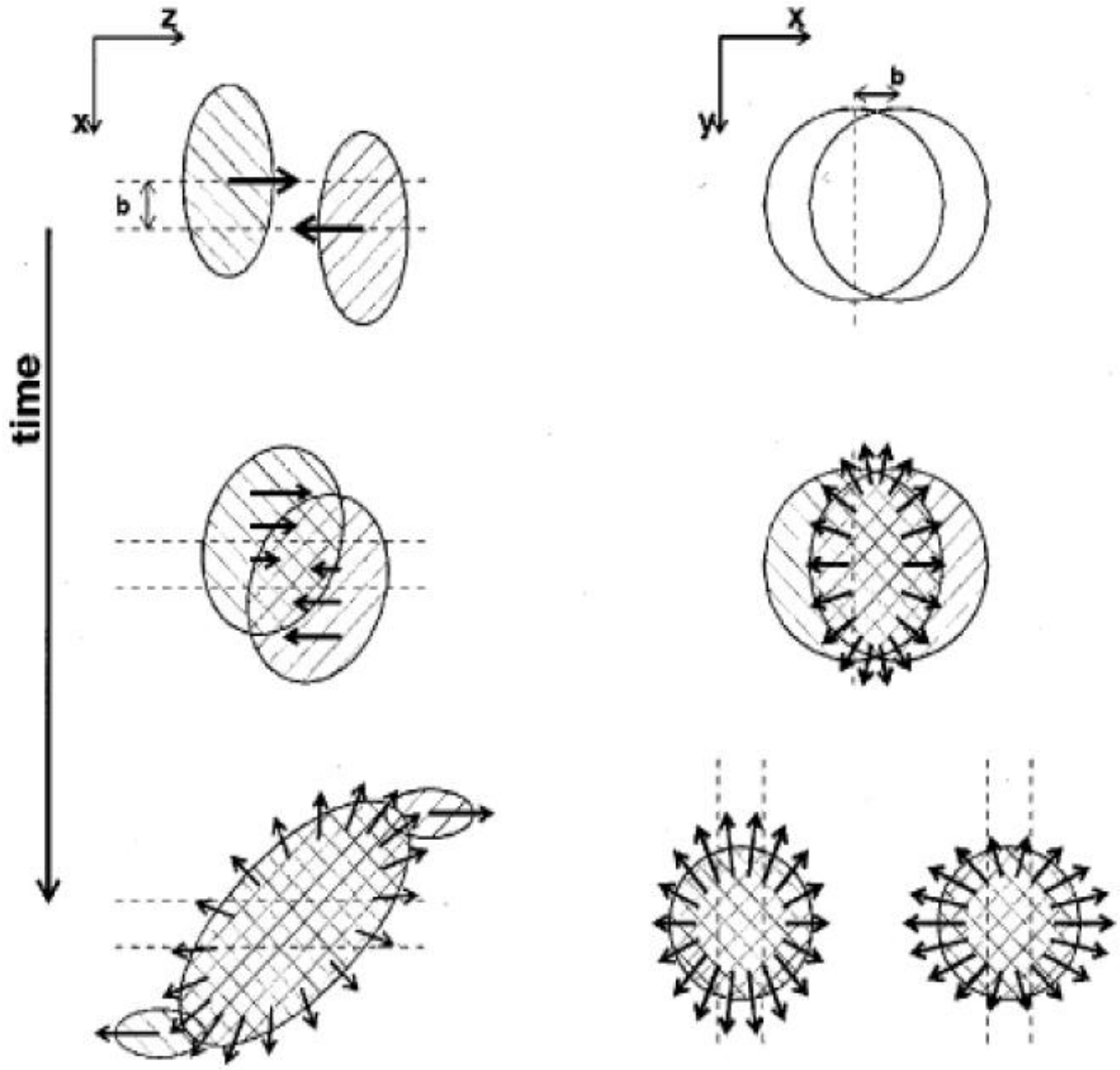

Fig 1.2: Schematic view of the time evolution in a heavy-ion collision. On the left, is the side view of the time evolution of the reaction and on the right is a sketch of the top view.

1.4 Nuclear Stopping

One of the important phenomenon which occurs at intermediate energy is nuclear stopping, which can be viewed as a measure of the degree to which the energy of the relative motion of the two colliding nuclei is transformed into other degrees of freedom. The amount of nuclear stopping determines the energy and volume of the interaction region, which govern the reaction dynamics and the extent to which conditions might be favourable for formation of a high density, deconfined phase of matter. Higher nuclear stopping will cause more thermalization of the system due to large number of violent collisions.

When two nuclei collide under certain conditions, the following scenarios are possible:

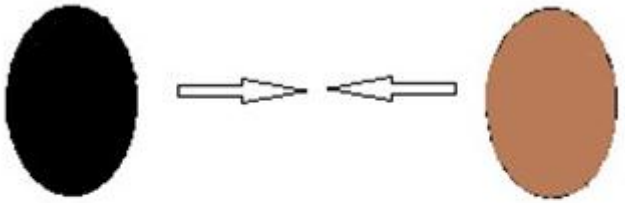

Fig. 1.3(a)

Fig. 1.3(b)

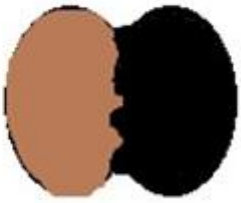

Fig. 1.3(c)

1) In the first case, the nuclei collide, and are repelled by each other as shown in Fig. 1.3 (a).
2) The two nuclei mix up like in the collisions of two compressible droplets as shown in Fig. 1.3 (b).
3) The nuclei pass each other without suffering any significant collisions or interactions as shown in Fig. 1.3(c).

The different scenarios explained above would result in different longitudinal and transverse momentum distributions for the projectile and target nuclei. Our interest in heavy ion collisions is represented by Fig.1.3 (b), which results in the phenomenon of global stopping. Global stopping is defined as the randomization of one-body momentum space or memory loss of the incoming momentum or momentum transfer during the break of the initial correlations among nucleons of projectile and target nuclei.

The colliding nuclei compress each other, increasing the density and thus heating the Baryon matter. The degree of compression and temperature will depend on the EOS of the system which relates the pressure to the density and temperature. The next stage of the reaction is the relaxation of the energy density, and the expansion of the composite system, thereby reducing the temperature and density. For central collisions, this expansion is symmetric. However, for collisions at finite impact parameter, the system expands into the direction of the largest gradients in density and temperature. Finally, the reaction and interactions between the colliding particles stops, at a point called 'freeze-out'.

All the above properties, like theramalization, equation of state and longitudinal and transverse momentum distributions of the colliding particles can be understood and visualised with the help of stopping parameters. More the initial memory of nucleons is lost or erased, more is the stopping and better will be the average mixing of projectile and target momentum. The degree of stopping depends significantly on incident energies, mass of colliding nuclei and colliding geometry.

One may conclude that a complete knowledge about the degree of stopping is very important in understanding the properties and dynamics of the colliding system, and providing new predictions which may be probed by experimentalists for further investigations.

In earlier attempts, a lot of work on nuclear stopping has been done both theoretically as well as experimentally. Zhang, *et al.* [16] gave a unified description of the nuclear stopping taking into account the parameter isotropy ratio, in central HIC's from 10 MeV/nucleon to 1.2 GeV/nucleon. Li and Li [17] studied the dependence of nuclear stopping Quadrupole moment $<Q_{ZZ}/A>$ and Anisotropy ratio $<R>$ in intermediate-energy heavy ion collisions on system size, initial *N/Z*, isospin symmetry potential, and medium corrections of two-body cross sections. They found the effect of the initial *N/Z* ratio, as well as isospin symmetry potential, is weak on stopping. The excitation function of Q_{ZZ}/A and *R*, however, depends on the form of the medium corrections of two-body cross-sections and on the EOS of nuclear matter. Liu, *et al.* [18] studied the nuclear stopping for various colliding systems with different neutron-proton ratios over large domains of incident energy and discovered that nuclear stopping is very sensitive toward the isospin content of in-medium nucleon-nucleon cross-section above Fermi energy. In another study by Kumar, *et al.* [19], a complete systematics (excitation function, impact parameter, system size, isospin asymmetry, and EOS dependences) of global stopping and fragment production for heavy-ion reactions in the energy range between 50 and 1000 MeV/nucleon, was carried out in the presence of symmetry energy and an isospin-dependent cross section. The study reveals that the degree of stopping depends weakly on the symmetry energy and strongly on the isospin-dependent cross section. Moreover, nuclear stopping and LCP's can be used as a tool to get the information about the isospin-dependent cross section.

In the present thesis, simulations are carried out for symmetric reactions in the energy range 90 MeV/nucleon – 1.5 GeV/nucleon using the isospin dependent quantum molecular dynamics (IQMD) model [20]. The influence of isospin dependent and isospin independent cross-sections is examined on the stopping parameter varxz (ratio of transverse and longitudinal momentum distributions) for fragment charge Z=1, 2, 3, 4. The isospin dependent cross section (σ_{iso}) reads as:

$$\sigma_{np} = 3\,\sigma_{nn} = 3\,\sigma_{pp}$$

And isospin independent coss-section ($\sigma_{no\ iso}$) is given by:

,

$$\sigma_{np} = \sigma_{nn} = \sigma_{pp}$$

The effect of three different clusterization algorithms (MST, MSTP, iso-MST) [21-23] is also noted on the stopping observable *varxz* in addition to various reaction parameters such as energy and impact parameter. The theoretical findings are compared to the experimental data wherever possible.

1.5 Review of Experimental Attempts

Some of the research facilities/institutes working in the intermediate energy scale.

1. BERKLEY [24-25]: The experiments performed in Berkley served to get the experimentalists aware of the problems from medium energy heavy-ion collisions to the equation of state. The Berkeley group focus mainly on the asymmetric reactions between the incident energy 50 to 110 MeV/nucleon, with an aim to investigate the role of entrance-channel mass asymmetry reaction dynamics. The emphasis was on the different parameters like excitation energy, angular distribution, cross-section as well as velocity distribution.
2. Michigan state university (USA) [26-28]: The MSU group at the National Superconducting Cyclotron Laboratory (NSCL) has been active in studying the fragment's spectra at lower side of the bombarding energies. For both symmetric and asymmetric reactions, the isospin effects are studied by neutron-proton spectra double ratio, cross-section and binding energy, rapidity distribution, transverse momentum and impact parameter dependence of isospin diffusion.
3. GANIL (France) [29]: The INDRA collaboration at GANIL has done extensive study on nuclear stopping in central collisions at intermediate energies in the range 40-100 MeV/nucleon. They investigated the behaviour of isotropy ratio in central symmetric nuclear reactions at intermediate energies and explored the isospin content of the system with respect to nuclear stopping.
4. GSI (Germany) [30]: the SIS (heavy ion synchrotron) accelerator is specifically designed to study heavy ion collisions at intermediate energies. The FOPI group at GSI studied the systematics of central heavy ion collisions in the 1 GeV/nucleon regime. The observables include cluster multiplicities, longitudinal and transverse rapidity distributions and stopping. The data is compared to earlier data and to transport model simulations.
5. The symmetric collisions are studied by the Superconducting Cyclotron (SC) and CHIMARA detector of the Laboratori Nationali del Sud of INFN (Italy) [31]. They have presented the multiplicity of LCP's and IMF's in peripheral and semi-peripheral collisions as a function of excitation energy of emitting source, mass of the system and beam energy.
6. The NIMROD collaboration focuses on the reaction dynamics in Fermi energy domain of the heavy-ion collisions. The study of equation of state of isospin asymmetric nuclear matter has also been studied by this collaboration. [32]

7. Other research facilities [14] include Relativistic Heavy-Ion Collider (RHIC) (USA), Superconducting Super-Collider (SSC) at BNL (USA), NSF-Arizon accelerator at the University of Arizona (USA), Vivitron Accelerator in Strasbourg (France), and Superconducting Cyclotron (SC) at Texas (USA).

1.6 Review of Various Theoretical Models

Over the years, several theoretical models have been developed to simulate and understand heavy ion collisions. The treatment of heavy ion collisions is not straight forward as it involves non-equilibrium physics. The whole dynamics at low energies is governed by the mean field or by the mutual two and three body interactions. Whereas, at higher energies, role of Pauli's principle becomes quite small, and the role of N-N collisions becomes significant. The dynamics at intermediate energies, however, requires equal weightage to nucleon-nucleon binary collisions and mean field. We now discuss few of these transport models briefly:

1.6.1 Time Dependent Hartree-Fock (TDHF) Theory[33]:

TDHF is a quantum mechanical theory which is used to describe the low energy heavy ion collisions. Its fundamental physical assumption is that the (well-established) independent particle behaviour for the near- equilibrium nuclear states persists to highly non-equilibrium situations if the excitation energy is less that 10 MeV/nucleon. Later, Attempts were made to extend TDHF to include NN collisions known as extended time dependent Hartree-Fock (ETDHF) equation. It was able to explain fusion, compound nucleus formation, dissipation, shock wave propagation, and fragmentation. However, due to complications, this theory could not be used for large scale investigations.

1.6.2 Intra Nuclear Cascade (INC) Model[34]:

In this model, mean field is completely neglected and nucleon-nucleon collisions are included without Pauli-blocking. It first simulates the heavy ion collisions as a superposition of independent two body NN collisions. Then, each nucleus is considered as a collection of point particles distributed within a sphere without any Fermi momentum. The position of each nucleon is assigned by Monte-Carlo sampling and the whole reaction time is divided into small intervals Δt. Two nucleons are

supposed to collide if they pass the point of closest approach within a given time interval. The distance of closest approach $d_{min} = [\sigma_{nn}(\sqrt{s}) /\pi]^{0.5}$ with σ_{nn} $(\sqrt{s})$ as the total nucleon-nucleon cross section in their centre of mass system and $\sqrt{s}$ the centre of mass energy. The INC model gave excellent opportunity to extract the information about several experimental observables. However, it is suitable for only high/intermediate energy experiments, as mean field is not included in this model.

1.6.3 Boltzmann-Uehling-Uhlenbeck (BUU) Model[35-36]:

It solves the BUU equation using test particle method. The phase space of each nucleon is represented by large number of pseudo- particles and these test particles are treated as classical point particles which are associated with Gaussian wave packet. The particles are then propagated under the classical Hamilton's equations of motion.

BUU model is able to explain one-body observables like collective flow, stopping, and particle spectra. But, Due to lack of fluctuations and correlations, the N-body predictions are beyond the scope of this model.

1.6.4 Quantum Molecular Dynamics (QMD)[8]:

The QMD model is an n-body theory which simulates heavy ion reactions at intermediate energies on an event by event method. Each event is simulated independent of other events. In contrast to BUU model, no averaging is done over various events and hence, the correlations among nucleons can be preserved. The nucleons are represented by Gaussian wave packets which interact by mutual two and three body forces. The successfully initialized nuclei are boosted towards each other using relativistic kinematics. The equation of motion of many-body system is, then calculated by means of generalized variational principle. The QMD model contains the following ingredients: short-range interaction (hard-core repulsion), stochastic scattering with energy and angle dependent cross sections, inelastic collisions and Fermi motion of the nucleons in the ground state as well as the consideration of the quantum effect of the Pauli principle. QMD is a microscopic description of heavy-ion collisions, similar to the Vlasov-like models of the preceding section (BUU model). The collisions in QMD are treated in the same way as in BUU model. Two particles undergo scattering if they are closer than a distance $[\sigma_{nn}(\sqrt{s}) /\pi]^{0.5}$. The effect of N-body collisions is found to be quite low and is thus neglected. The scattering is further

checked for the fulfilment of Pauli- principle. The collisions which violate the Pauli principle are neglected. Whenever a collision occurs, the phase space around these scattering centres is checked. Each nucleon is assumed to occupy a sphere in coordinate and momentum space. This yields the same Pauli blocking ratio as an exact calculation of the overlap of the Gaussians will yield. Several refinements and improvements were made over the original QMD, and the new versions were named as BQMD, IQMD, HQMD, etc. In this thesis, we shall confine to IQMD (Isospin dependent QMD), which includes the isospin effects of the system.

.

1.7 Summary

A detailed and systematic study of heavy ion collisions at intermediate energy scale provides us with information about the bulk properties of nuclear matter which is used to understand phenomena like origin of early universe and supernova explosions etc. Some of the important processes taking place in this energy regime include multifragmentation, nuclear flow, and nuclear stopping which are discussed briefly in this chapter. Since the present thesis deals with nuclear stopping and its analysis, the reader is introduced to a brief review of both theoretical as well as experimental attempts. Over the years, various theoretical models have been used to simulate and describe the nuclear processes in intermediate energy regime, including Time Dependent Hartree-Fock (TDHF) Theory, Intra Nuclear Cascade (INC) Model, and Quantum Molecular Dynamics (QMD). An improvement over QMD which includes the isospin nature of the nucleons has been developed, termed as Isospin Dependent Quantum Molecular Dynamics (IQMD). The present work is done within the framework of IQMD model that will be discussed in detail in the next chapter.

Chapter 2

METHODOLOGY

As discussed in chapter 1, dynamics of heavy ion collisions can be studied by various phenomena. The isospin dependent effects such as symmetry energy, isospin dependence of nucleon-nucleon cross-section, etc. can be studied by incorporating isospin effects into the model. The isospin version of QMD is known as Isospin dependent Quantum Molecular Dynamics (IQMD). The following section explains this model in detail.

2.1 IQMD[20]

The Isospin dependent Quantum Molecular Dynamics (IQMD) treats the different charge states of nucleons, deltas and pions explicitly. The isospin degrees of freedom enter into the model via both cross-sections and mean field. This model includes three steps: first, the nuclei have to be generated under certain conditions. This procedure is called as *initialization*. The generated nuclei have to be propagated under the influence of surrounding mean field, termed as *propagation*. Finally, nucleons are bound to collide if they come too close to each other. This part is dubbed as *collisions*. The elastic and inelastic cross-sections for proton-proton, neutron-neutron as well as proton-neutron are supposed to be affected in the presence of isospin.

a) Initialization: Nucleons are represented by Gaussian wave packets which interact by mutual two and three body forces. Each nucleon is represented by a coherent state of the form:

$$f_i(r,p,t) = \frac{1}{\pi^2\hbar^2} e^{-(r-r_i(t))^2\frac{1}{2L}} e^{-(p-p_i(t))^2\frac{2L}{\hbar^2}} \quad (1)$$

Where the Gaussian width L represents the interaction range of particle. The system dependence of L has been introduced in IQMD in order to obtain maximum stability of the nucleonic density profiles. For the heavier system (e.g. Au + Au), its value is chosen 8.66 fm^2, while for lighter one (i.e. Ca + Ca), the value is 4.33 fm^2. Nucleons are initialized in a sphere with radius $R=1.12A^{1/3}$fm, in accordance with the liquid drop

model. The initial momenta are randomly chosen between 0 and Fermi momentum (P_F), without any further local constraints.

The total *n*-body wave function is then assumed to be the direct product of coherent states:

$$\Phi = \Pi_i f_i(r_i, p_i , t) \quad (2)$$

The stability of the nucleus generated using IQMD can be checked by referring to the radius and momentum at different time scales (Fig. 2.1 and 2.2):

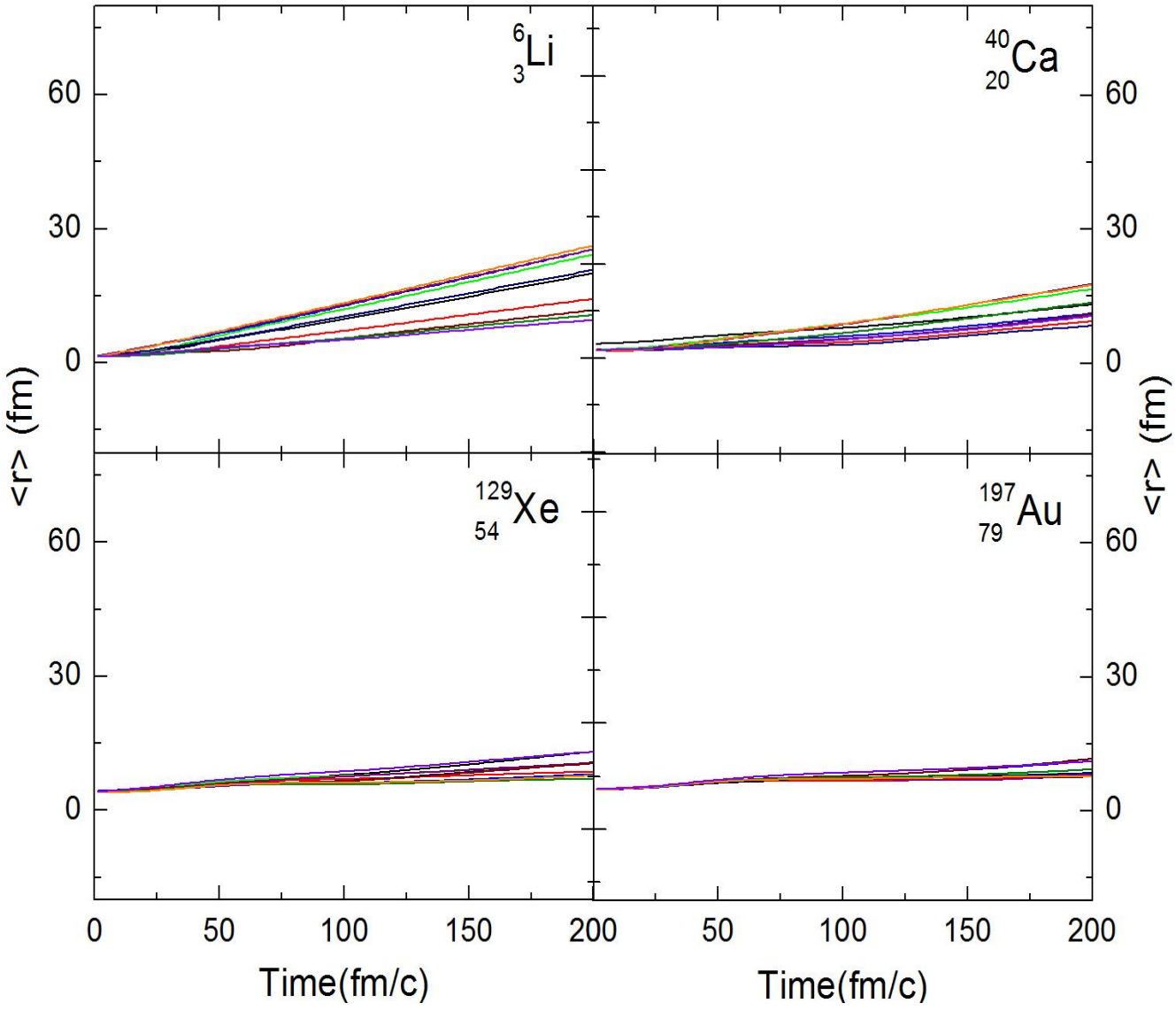

Fig 2.1: Evolution of the nuclear radius for different nuclei. The different coloured times represent the different initializations by IQMD model.

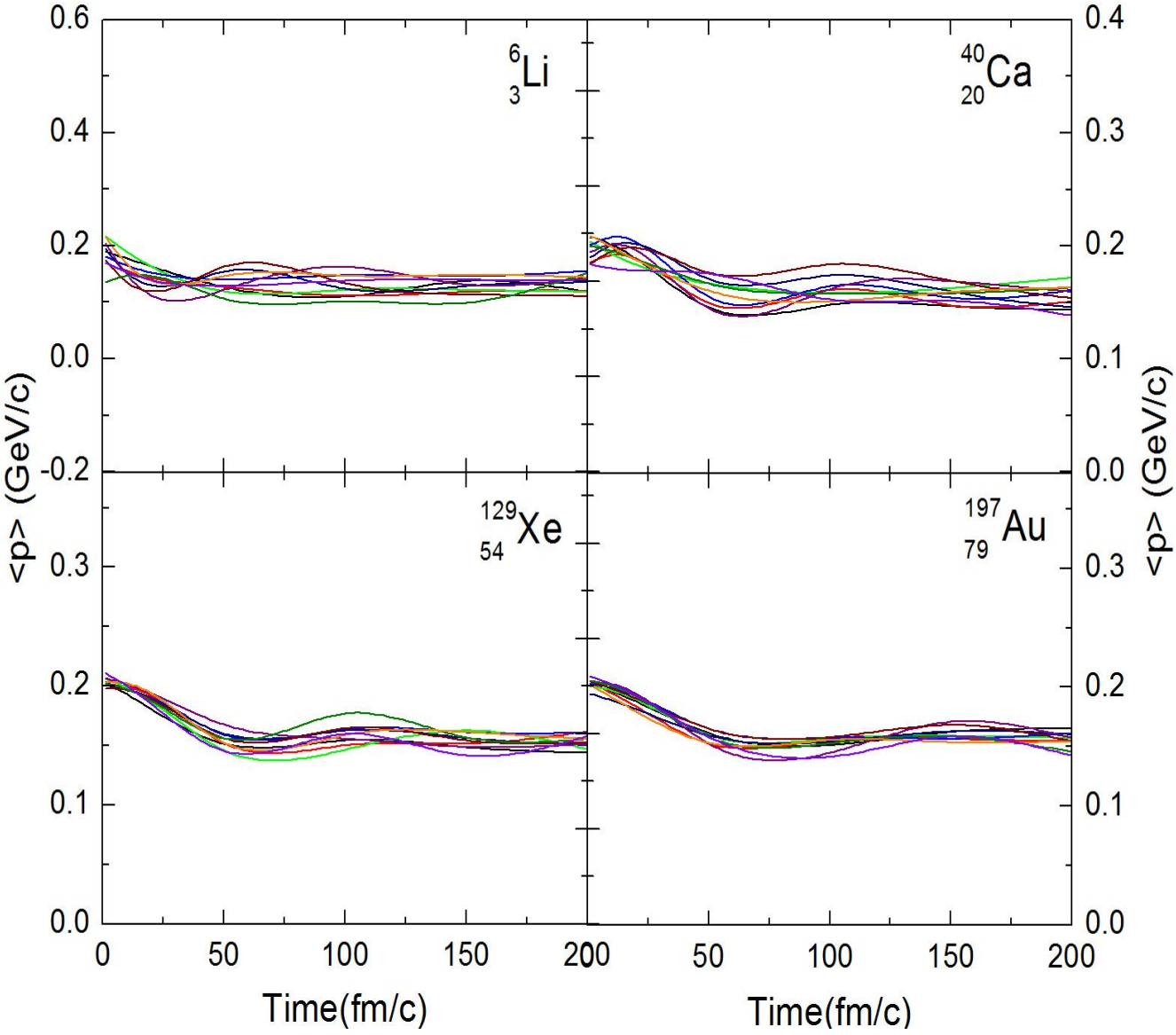

Fig 2.2: Evolution of momentum for different nuclei. The different coloured times represent the different initializations by IQMD model.

From Figs. 2.1 and 2.2, it can be seen that for 10 different initializations in the IQMD simulation, the radius and momentum quantities remain fairly stable till 200 fm/c. This proves that the IQMD model is suitable for generating the appropriate nuclei for our analysis.

b) Propagation: The successfully initialized nuclei are boosted towards each other using relativistic kinematics. The equation of motion of many-body system is, then calculated by means of generalized variational principle. This process includes first setting the Lagrangian of the system:

$$L = \langle \varphi | i\hbar \frac{d}{dt} - H | \varphi \rangle \tag{3}$$

Since the action should be stationary under the allowed variation of the wave function:

$$\delta S = \delta \int_{t1}^{t2} L[\phi, \phi *] d\tau = 0 \tag{4}$$

For the coherent states and a Hamiltonian of the form $H = \Sigma_i T_i + \frac{1}{2}\Sigma_{ij} V_{ij}$, the Lagrangian and the variation can easily be calculated. The hadrons propagate using Hamilton's equations of motion:

$$\frac{dr_i}{dt} = \frac{d\langle H \rangle}{dp_i} \tag{5}$$

$$\frac{dp_i}{dt} = -\frac{d\langle H \rangle}{dr_i} \tag{6}$$

With,

$$\begin{aligned} \langle H \rangle &= \langle T \rangle + \langle V \rangle \\ &= \sum_i \frac{p_i^2}{2m_i} + \sum_i \sum_{j>i} \int f_i(r,p,t) V^{ij}(r',r) \\ &\quad \times f_j(r',p',t) dr dr' dp dp' \end{aligned} \tag{7}$$

The total potential in equation (7) reads as:

$$\begin{aligned} V^{ij}(r'-r) &= V^{ij}_{Skyrme} + V^{ij}_{Yukawa} + V^{ij}_{Coul} + V^{ij}_{mdi} + V^{ij}_{sym} \\ &= \left(t_1 \delta(r'-r) + t_2 \delta(r'-r) \rho^{\gamma-1} \left(\frac{r'+r}{2} \right) \right) \\ &\quad + t_3 \frac{exp(|r'-r|/\mu)}{(|r'-r|/\mu)} + \frac{Z_i Z_j e^2}{|r'-r|} \\ &\quad + t_4 \ln^2 [t_5 (p_i' - p)^2 + 1] \delta(r'-r) \\ &\quad + t_6 \frac{1}{\varrho_0} T_3^i T_3^j \delta(r_i' - r_j). \end{aligned} \tag{8}$$

Where Z_i and Z_j denote the charges of the i^{th} and j^{th} baryon, and T_3^i and T_3^j are their respective T_3 components (i.e., 1/2 for protons and -1/2 for neutrons). The IQMD-model offers rather stable density distributions and good energy conservation, however at the price of nucleon evaporation and improper binding energies ($E_{bind} \approx$ 4-5 MeV/nucleon for heavy nuclei instead of 8 MeV/nucleon). A symmetry potential between protons and neutrons corresponding to the Bethe-Weizsäacker mass formula has been included:
Other baryonic potentials like V_{ij}^{Skyrme} and V_{ij}^{mdi} are defined isospin independent like in all other flavors. The Yukawa potential in IQMD V_{ij}^{Yuk} is very short ranged (μ = 0.4 fm in contrast to μ = 1.5 fm in QMD) and weak. Yukawa forces stabilize the nuclei because of the increase of the interaction range as compared to a δ-like Skyrme-potential. Thus nucleons notice earlier that they will arrive at the surface and are more effectively decelerated as without this potential. In addition the fluctuations are reduced.

The nucleons close to the surface are unbound initially as the local potential is low, which results in a reduced binding energy per nucleon as compared to Weizsäacker mass formula. Hence the initialized nuclei are less stable against spurious particle evaporation as compared to QMD. On the other hand this approach makes available the full Fermi-energy calculated from the Skyrme ansatz. Also IQMD performs a Lorentz contraction of the nucleus coordinate distribution which is not present in QMD and which becomes important for higher energies *Energy/nucleon* > 1 GeV.

In IQMD the centroids of the Gaussians in a nucleus are randomly distributed in a phase space sphere ($r < R$ and $p < p_F$) with $R = 1.12A^{1/3}$ fm corresponding to a ground state density of $\rho_0 = 0.17$ fm^{-3}. The Fermi momentum p_F depends on the ground state density. In QMD the maximum momentum is determined by the local binding energy (which causes an effective reduction of the total Fermi energy to about 10 – 12 MeV), whereas in IQMD the momenta are uniformly distributed within a momentum sphere $p \leq p_F$ without further local constraints.

c) Collision: Finally, two nucleons will suffer a binary collision if the distance between their centroids equals:

$$|r_i - r_j| \leq \sqrt{\frac{\sigma_{tot}}{\pi}}, \sigma_{tot} = \sigma(\sqrt{s}, type) \tag{9}$$

Where 'type' in the above equation denotes the in-going collision partners (N-N, N-Δ, N-π, etc.). Similar to QMD model, In IQMD, the scattering is further checked for the fulfilment of Pauli- principle. The collisions which violate the Pauli principle are neglected.

Whenever a collision occurs, the phase space around then scattering is checked. Each nucleon is assumed to occupy a sphere in coordinate and momentum space. This yields the same Pauli blocking ratio as an exact calculation of the overlap of the Gaussians will yield. The fractions P_1 and P_2 of final phase spaces for each of the two scattering partners that is already occupied by other nucleons, is calculated. The collision is blocked with a probability:

$$P_{block} = 1 - (1 - P_1)(1 - P_2) \qquad (10)$$

The difference between IQMD and QMD becomes clear from the following figure:

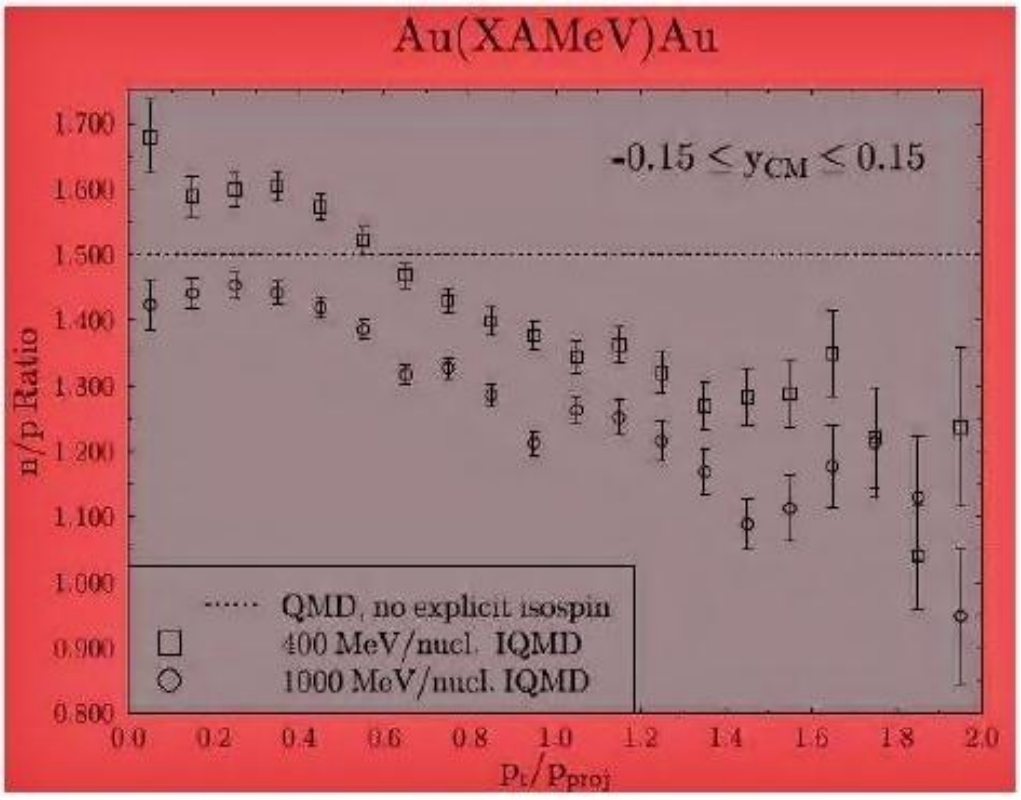

Fig. 2.3: Ratio of free neutron to free protons versus transverse momentum pt at midrapidity for Au + Au collision between 3 and 9 fm impact parameter at 400 and 1000 MeV/nucleon incident beam energy. [14]

From Fig. 2.3, it is seen that n/p ratio for the QMD case remains constant at 1.5 independent of transverse momentum and incident beam energy. Whereas, IQMD results show a decrease in neutron to proton ratio with increasing transverse momentum due to Coulomb interactions. Apart from the p_t dependence, a strong dependence on the incident energy is also observed. Due to the explicit inclusion of isospin, the n/p ratio decreases with increasing beam energy.

In Figs. 2.4 and 2.5, one can see the collision dynamics reproduced by IQMD at two different impact parameters.

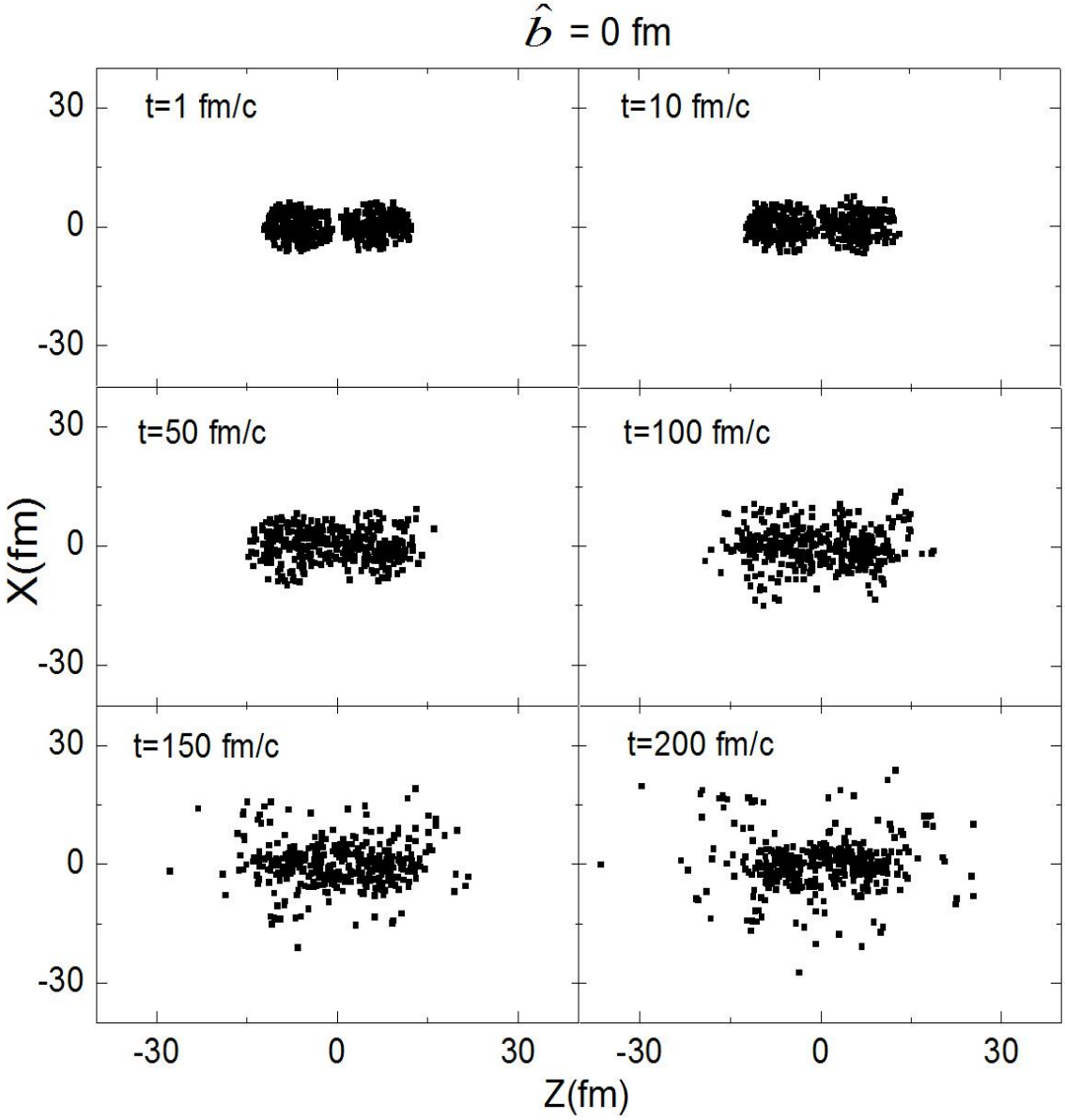

Fig. 2.4: Coordinate space for $^{197}_{79}$Au + $^{197}_{79}$Au collision at impact parameter $\hat{b}$ = 0 fm.

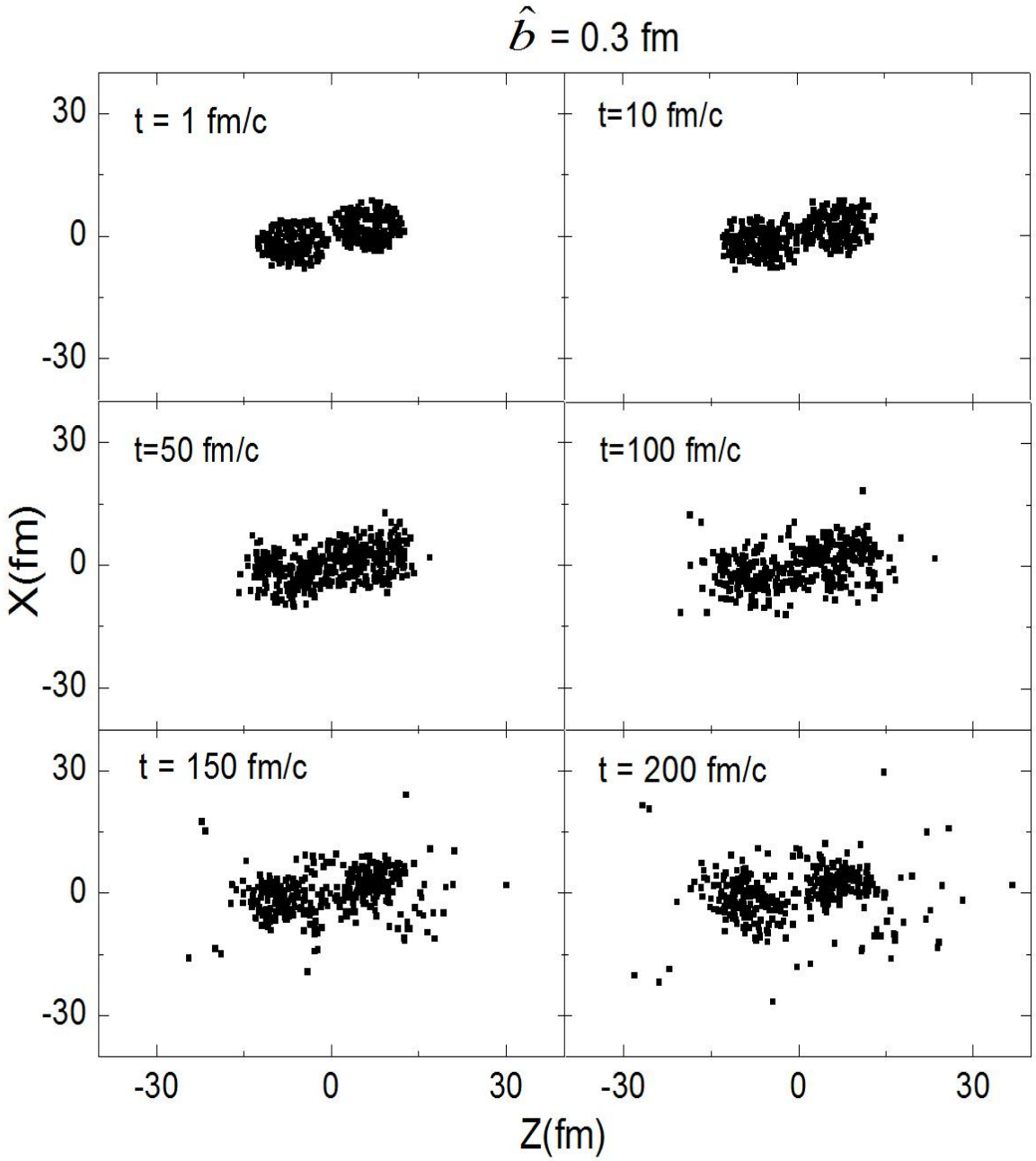

Fig. 2.5: Coordinate space for $^{197}_{79}$Au + $^{197}_{79}$Au collision at impact parameter $\hat{b}$ = 0.3 fm.

From figs. 2.4 and 2.5, which show the coordinate space of the nucleons; one can see that the reaction dynamics and fragmentation is governed by the impact parameter used in the IQMD model.

The following figure (Fig. 2.6) represents the momentum space of the reaction plane for $\hat{b}$ = 0 fm.

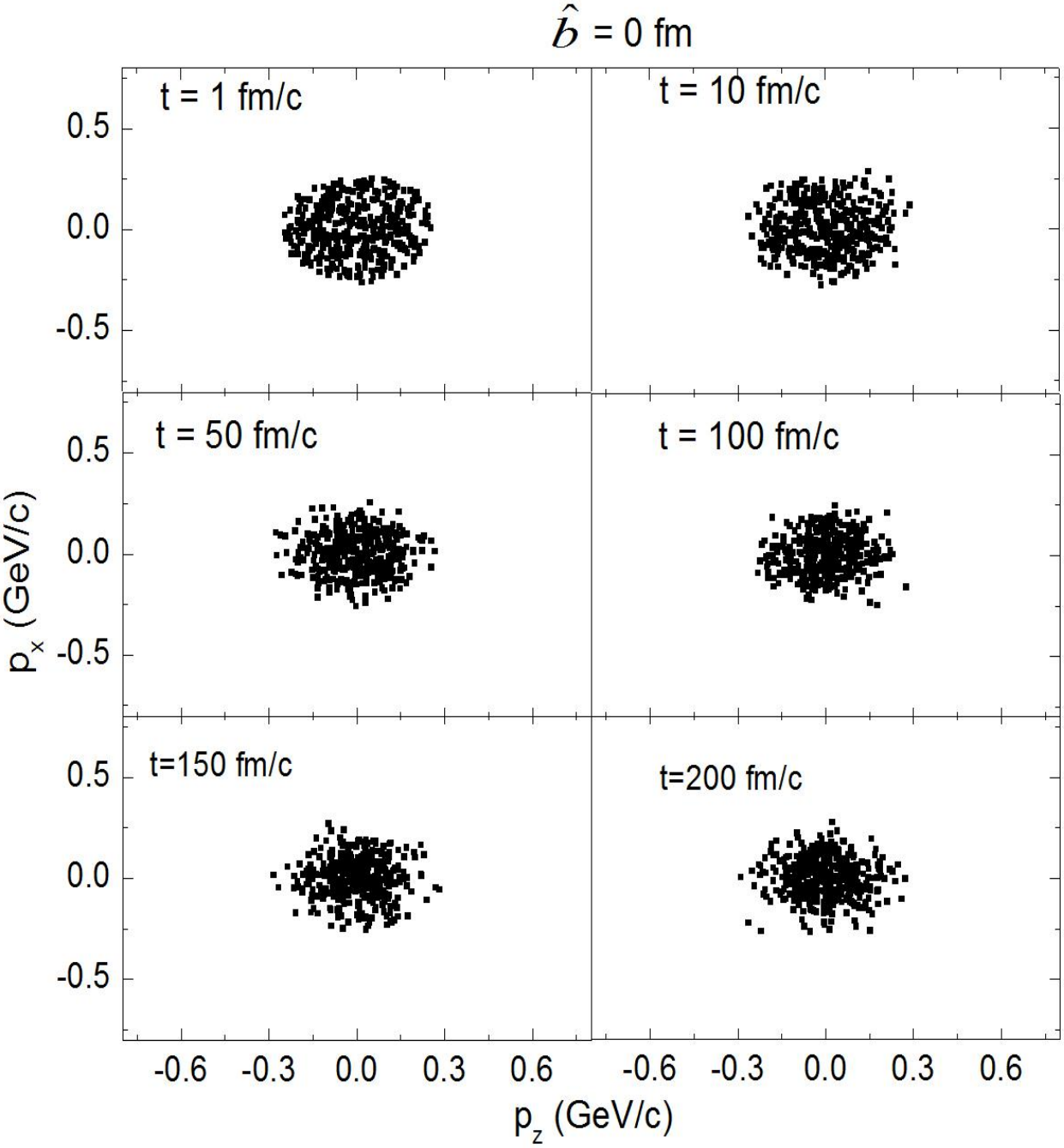

Fig. 2.6: Momentum space for $^{197}_{79}$Au + $^{197}_{79}$Au collisions at impact parameter $\hat{b}$ = 0 fm.

2.2 SECONDARY MODELS: METHODS OF CLUSTERIZATION

Once the phase space is generated by the IQMD model, we need to clusterize or group the different particles in the form of fragments according to various conditions. This is done through different clusterization algorithms. These algorithms impose constraints on the relative distance or momentum (or both) between two particles and form a fragment accordingly. In this dessertation, we will confine ourselves to only three clusterization techniques/algorithms which are discussed below in brief.

2.2.1 Minimum Spanning Tree (MST) [21]: In MST method, two nucleons share the same fragment if their centroids are closer than a distance d_{min},

$$|r_i - r_j| \leq d_{min} \tag{11}$$

Where r_i and r_j are the spatial positions of both nucleons. The value of d_{min} can vary between 2-4 fm. In the present thesis, a value of 4 fm has been used.

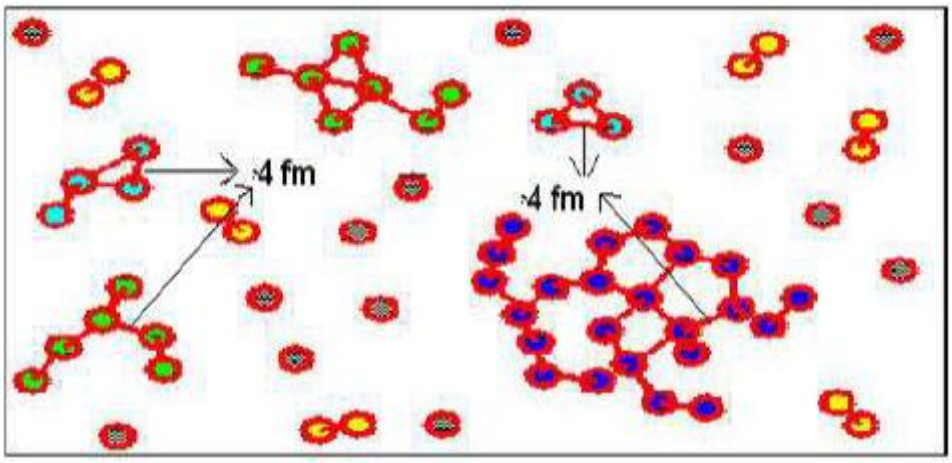

Fig. 2.7: Fragment production using MST method where distance between nucleons is $\leq d_{min}$ (4 fm)

This method cannot address the question of time scale as it will give a big fragment during the early stage of the reaction where the density is quite high and the interactions between the nucleons are still active. Moreover, inaccuracies may occur, because in the momentum space, the particles of the fragment may have different momenta. This is solved using the MSTP method discussed in the next section.

2.2.2 Minimum Spanning Tree with Momentum Constraint (MSTP) [22]: An improvement over the MST algorithm is to put additional constraint in momentum space. It

will help to get rid of fragments that although close in spatial space are far in momentum space. The MSTP method puts restriction on the spatial as well as momentum space of the nucleons. Nucleons will thus share a fragment if both the following conditions are followed:

$$|r_i - r_j| \leq d_{min} \quad (12)$$

$$|p_i - p_j| \leq p_{min} \quad (13)$$

This value of cut in the relative momentum of the two nucleons is about the average Fermi momentum of nucleons.

2.2.3 Minimum Spanning Tree with Isospin Cut (Iso-MST) [23]: The Iso-MST is a further modification of the MST algorithm, in which the Isospin nature of the nucleons is considered while imposing the constraint between two nucleons. The following conditions are obeyed by the nucleons of a fragment:

$$|r_{p1} - r_{p2}| \leq 3 \text{ fm} \quad (14)$$

$$|r_{n1} - r_{n2}| \leq 6 \text{ fm} \quad (15)$$

and

$$|r_{n1} - r_{p2}| \leq 6\text{fm} \quad (16)$$

Where n, p denote the neutron and proton of the fragment.

For comparison of the above mentioned clusterization methods, it has been observed from ref [23], that the momentum correlation methods recognize the fragments between 60– 100 fm/c, whereas the simple spatial-correlation method needs a much longer time. The response of a larger nucleon–nucleon cross section as well as of momentum-dependent interaction depends on the clusterization algorithm one is using. It is maximal with the spatial correlation method, whereas it is minimal with the energy minimization method. In addition, the spatial correlation with the inclusion of isospin dependence suppresses the yield of emitted nucleons and enhances the production of heavier fragments.

2.3 Summary

Summarizing, the Isospin Dependent Quantum Molecular Dynamics (IQMD) model is described in detail in which the isospin degrees of freedom enter into the model via both cross-sections and mean field. This model includes three steps: initialization, propagation, collisions. The isospin nature enters in both elastic and inelastic cross-sections for proton-proton, neutron-neutron as well as proton-neutron. The stability of the nuclei generated by IQMD is checked via the time evolution graphs of radius and momentum, done for various systems. The time evolution of coordinate and momentum space for $^{197}_{79}$Au + $^{197}_{79}$Au collisions is also checked for two different impact parameters, proving the IQMD model to be an appropriate approach for describing heavy ion collisions. Next, under the section, Secondary models, various clusterization methods are discussed briefly.

Chapter 3

NUCLEAR STOPPING IN HEAVY ION COLLISIONS

The nuclear stopping is defined as the percentage change in the kinetic energy of projectile nucleons in the nucleus-nucleus collision. It can be viewed as a measure of the degree to which the energy of the relative motion of the two colliding nuclei is transformed into other degrees of freedom [37]. The amount of nuclear stopping determines parameters, such as the energy and volume of the interaction region (and therefore energy density), which govern the reaction dynamics and the extent to which conditions might be favourable for formation of a high density, deconfined phase of matter. Therefore, an understanding of nuclear stopping measurements at the presently available collision energies should provide insight into the energy and baryon densities.

One of the main objectives for studying nuclear stopping is that it can be used as a probe to extract the information on the isospin dependence of in-medium nucleon-nucleon cross-section in intermediate energy heavy ion collisions. The study of the isospin effect at intermediate energy heavy ion collisions can be used to get the information for the in-medium nucleon-nucleon (*NN*) cross section and isospin dependent mean field. Another major goal in studying nuclear stopping is to investigate the reaction mechanisms of multi-fragmentation, flow, and the degree of thermalization achieved.

Over the years, efforts have been made to analyse the nuclear stopping in HIC's. In the literature [14], production of LCP's has been considered as an indicator to nuclear stopping and the degree of thermalization reached in the reaction. Other means include, studying the rapidity distribution of the longitudinal and transverse momenta of the nucleons, quadrupole moment, anisotropy ratio, and *varxz*, which are explained in the next section.

3.1 Parameters for Describing Nuclear Stopping

The following quantities can be used to describe nuclear stopping in HIC's [20]:

3.1.1 Quadrupole moment [17]

Quadrupole moment is defined as:

$$\langle Q_{ZZ} \rangle = \sum_i^A [2P_z^2(i) - P_x^2(i) - P_y^2(i)] \quad (17)$$

Where P_x, P_y contribute to the transverse momentum and P_z represents the longitudinal momentum. Here the total mass A is the sum of the projectile mass A_P and the target mass A_T. From Eqn. (18), one can see that Quadruple moment $\langle Q_{ZZ} \rangle$ vanishes for spherical distribution of momentum.

3.1.2 Anisotropy Ratio [17]

It is defined as the ratio of transverse to the longitudinal momentum:

$$\langle R \rangle = \frac{2}{\pi} \left(\frac{\sum_i^A |P_\perp(i)|}{\sum_i^A |P_{||}(i)|} \right) \quad (18)$$

The values of the transverse and longitudinal components of the momentum for the i^{th} nucleon are

$$P_\perp(i) = \{P_x^2(i) + P_y^2(i)\}^{1/2} \quad (19)$$

and

$$P_{||}(i) = P_z(i) \quad (20)$$

respectively. Naturally for a complete stopping, $\langle R \rangle$ ratio should be close to unity.

3.1.3 Rapidity Distribution [8]

Since stopping is a measure of the efficiency of converting the incoming longitudinal energy of a projectile and target into transverse degree of freedom (hence slowing down the incoming nucleons), the degree of stopping is thus given by rapidity distribution which reads as:

$$Y(i) = \frac{1}{2} \ln \frac{E(i)+P_z(i)}{E(i)-P_z(i)} \tag{21}$$

Where E(i) and P_z(i) are respectively, the total energy and longitudinal momentum of the i^{th} particle.

A symmetric central collision with a high degree of stopping can be viewed as a thermalized fireball sitting at rest in the c.m. frame, i.e. at midrapidity. For complete stopping, one should expect a single Gaussian shape of the rapidity. Obviously, narrow Gaussian indicates better thermalization compared to broader Gaussian.

3.1.4 varxz [30]

varxz is defined as the ratio of transverse to the longitudinal variances:

$$varxz = \frac{varx}{varz} = \frac{\sigma^2(x)}{\sigma^2(z)} \tag{22}$$

Where *varx* and *varz* are the variances obtained from the *fwhm* (full width at half maxima) of the rapidity distribution along transverse and longitudinal directions respectively from the relation:

$$fwhm = 2.36 * (var)^{1/2} \tag{23}$$

This definition of stopping has been adopted by INDRA and ALLADIN collaborations as well as the FOPI collaboration. [30]

Naturally, more the value of *varxz*, higher is the stopping achieved, and a value of unity will indicate full stopping. The present thesis shall take *varxz* as a parameter to analyse stopping for the various simulations carried out.

3.2 Results and Discussion

In the present work, simulations are carried out for symmetric reactions $^{40}_{20}$Ca +$^{40}_{20}$Ca, $^{58}_{28}$Ni +$^{58}_{28}$Ni, $^{129}_{54}$Xe +$^{129}_{54}$Xe, and $^{197}_{79}$Au + $^{197}_{79}$Au in the energy range 90 MeV/nucleon – 1.5 GeV/nucleon using the isospin dependent quantum molecular dynamics (IQMD) model. A scaled impact parameter $\hat{b} = b/b_{max}$ has been used where $b_{max} = 1.15(A_T^{1/3} + A_P^{1/3})$ fm (A_T and A_P are the mass of target and projectile respectively). The influence of different clusterization algorithms (MST, MSTP, iso-MST) on the stopping parameter *varxz* for fragment charge Z=1, 2, 3, 4, is examined. In addition to this, the effect of isospin dependent cross-section (σ_{iso}) and isospin independent cross-section ($\sigma_{no\ iso}$) is also investigated on *varxz* and the analysis is done for different energies, impact parameter, system mass and fragment charge. The theoretical findings are compared to the experimental data of FOPI collaboration. [30]

3.2.1 Phase Space Distribution

Figs. 3.1 and 3.2, show the co-ordinate space distributions of projectile and target for the system $^{197}_{79}$Au +$^{197}_{79}$Au. Figs. 3.1(a) and 3.1(b) denote the space distributions at incident energies 50 and 200 MeV/nucleon at scaled impact parameter $\hat{b}$ = 0 and Figs. 3.2(a) and 3.2(b) denote the same for $\hat{b}$ = 0.4 and 0.8 respectively. The left panel shows the rapidity distribution for isospin dependent cross-section (σ_{iso}) and right panel shows the rapidity distribution for isospin independent cross-section ($\sigma_{no\ iso}$). From fig. 3.1(a), one can observe that the final coordinate distribution (at t = 200 fm/c) in case of σ_{iso} is more spherical as compared to the case of $\sigma_{no\ iso}$. Therefore, indicating more stopping for isospin dependent cross-section. As the incident energy increases (Fig. 3.1(b)), the final distribution no longer remains spherical for both σ_{iso} and to $\sigma_{no\ iso}$, which gives indication that the influence of isospin dependence of the nucleon-nucleon cross-section decreases with increase in incident energy. As a next step, it can be seen that the effect of cross-section decreases as impact parameter increases (Figs. 3.2(a) and 3.2(b)). This is because the participant zone (which is the main contributor for nuclear stopping) decreases with impact parameter, resulting in a non-spherical distribution.

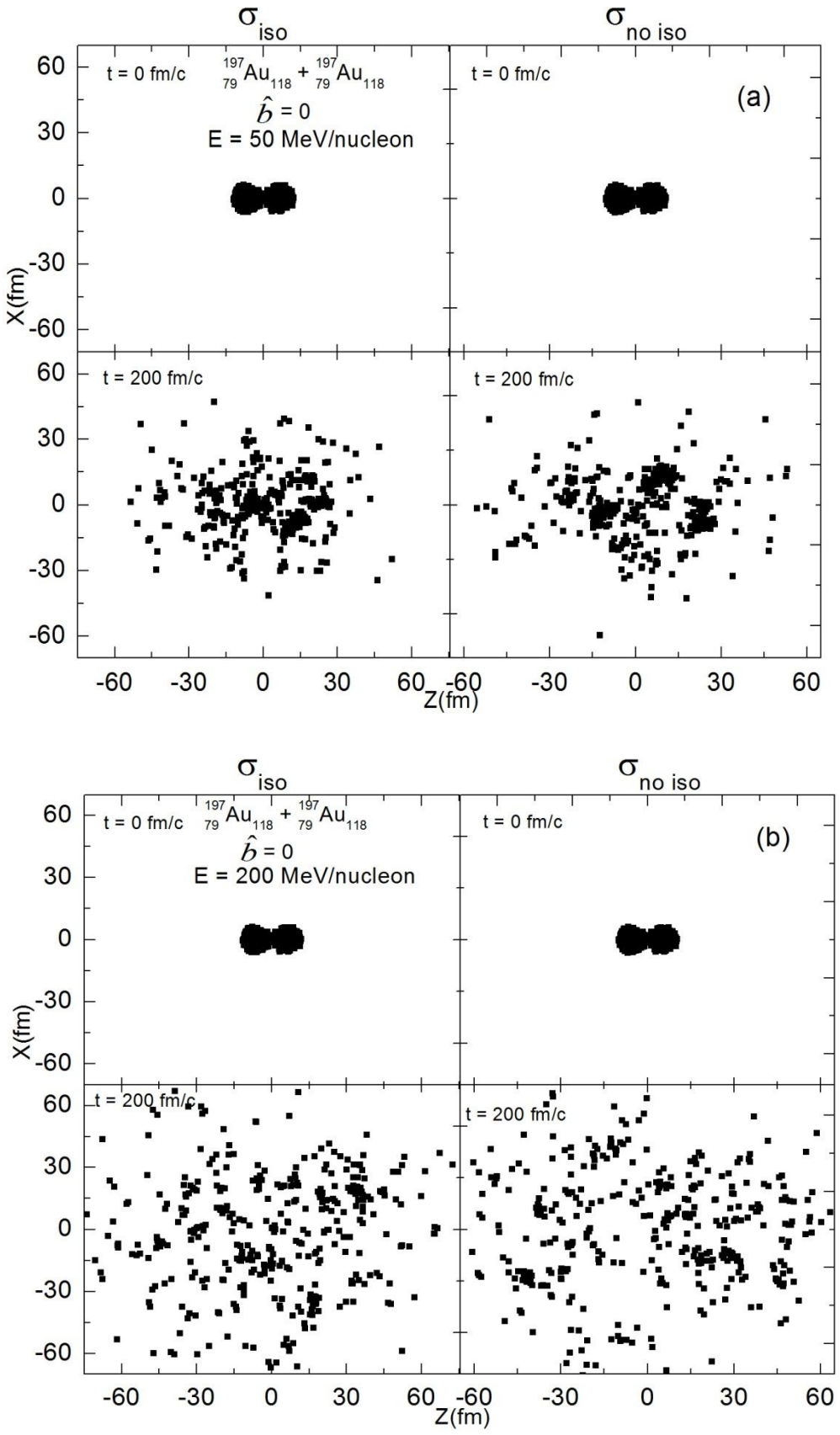

Fig. 3.1(a), (b): Coordinate space distribution for $^{197}_{79}$Au + $^{197}_{79}$Au at $\hat{b}$ = 0 fm and incident energy 50 and 200 MeV/nucleon, with σ_{iso} and $\sigma_{no\ iso}$

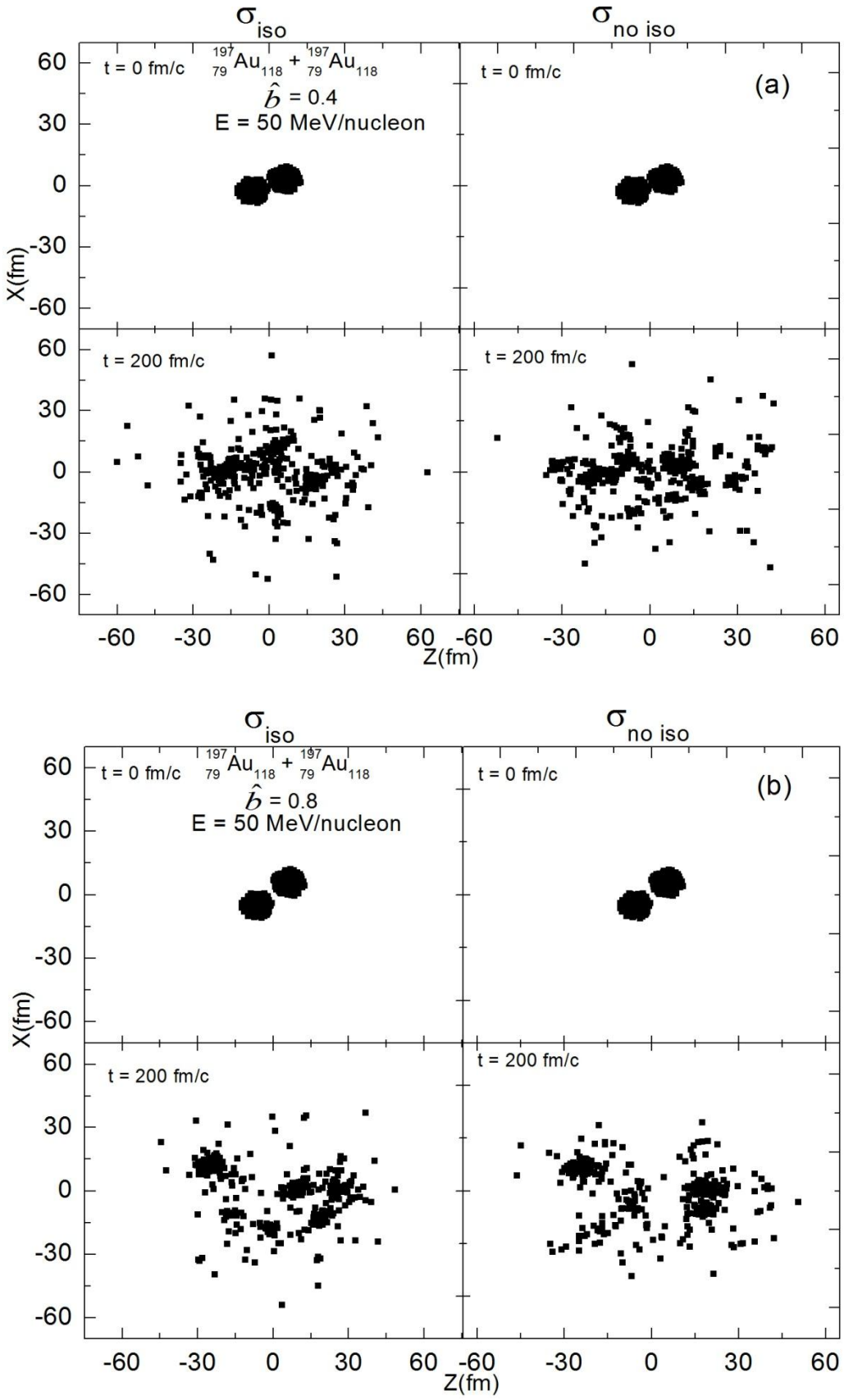

Fig. 3.2(a), (b): Coordinate space distribution for $^{197}_{79}Au + ^{197}_{79}Au$ at $\hat{b}$ = 0.4 fm and 0.8 fm and incident energy 50 MeV/nucleon, with σ_{iso} and $\sigma_{no\ iso}$

3.2.2 Rapidity Distribution

Figs.3.3 to 3.6 display the rapidity distribution as a function of $Y_{c.m}/Y_{beam}$ for symmetric systems $^{40}_{20}Ca + ^{40}_{20}Ca$, $^{58}_{28}Ni + ^{58}_{28}Ni$, $^{129}_{54}Xe + ^{129}_{54}Xe$, and $^{197}_{79}Au + ^{197}_{79}Au$ at an incident energy of 150 MeV/nucleon. Again, left panel shows the rapidity distribution for isospin dependent cross-section (σ_{iso}) and right panel shows the rapidity distribution for isospin independent cross-section ($\sigma_{no\ iso}$). The panels from top to bottom display the results for different clusterization algorithms namely MST, MSTP and iso-MST. It is observed that the longitudinal distributions are broader than the corresponding transverse distributions. And, the lighter systems show a broader Gaussian than the heavier ones, indicating more thermalization and hence a higher stopping in the heavier systems. In general, one can conclude that isospin effects of the cross-section do not play any significant role in influencing the rapidity distribution peaks, although the ratio of the variances of the transverse and longitudinal rapidities may differ in each case, thereby affecting the stopping. Moreover, the different clusterization techniques influence the Gaussian distribution only slightly.

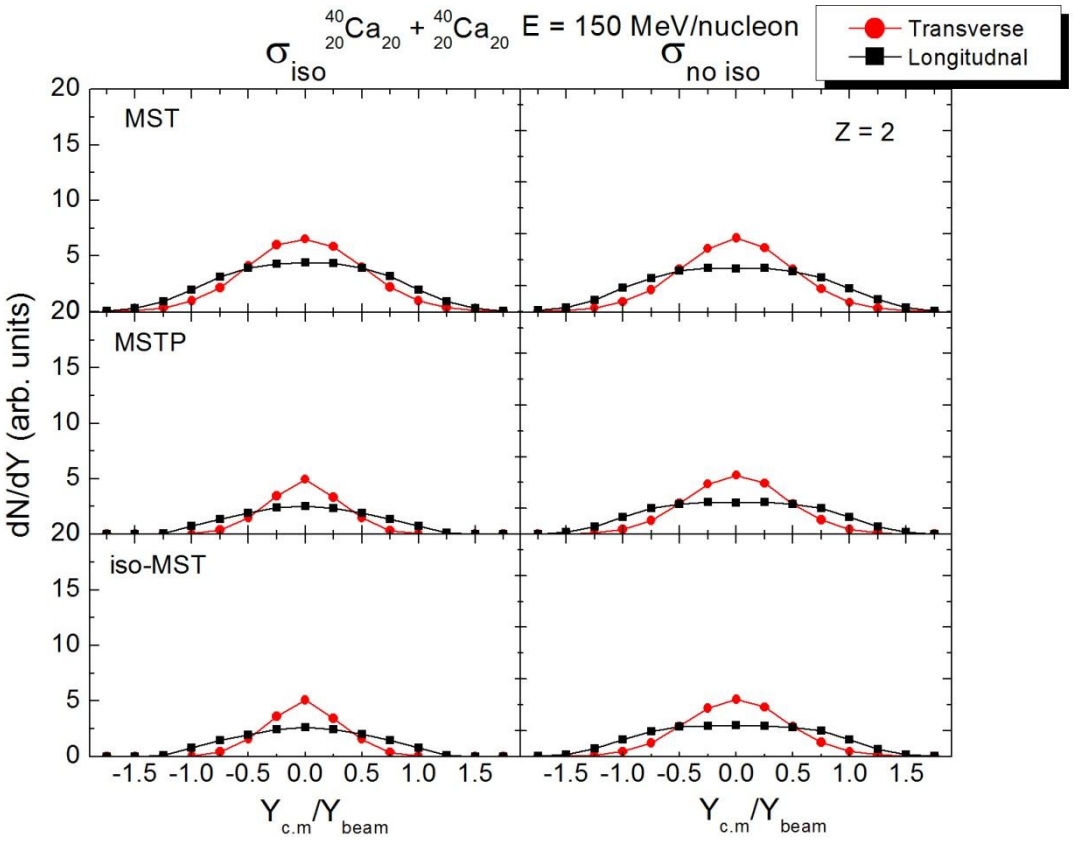

Fig. 3.3: Rapidity distribution as a function of $Y_{c.m}/Y_{beam}$ for $^{40}_{20}Ca + ^{40}_{20}Ca$, system at $\hat{b}$ = 0 fm and incident energy 150 MeV/nucleon, with σ_{iso} and $\sigma_{no\ iso}$

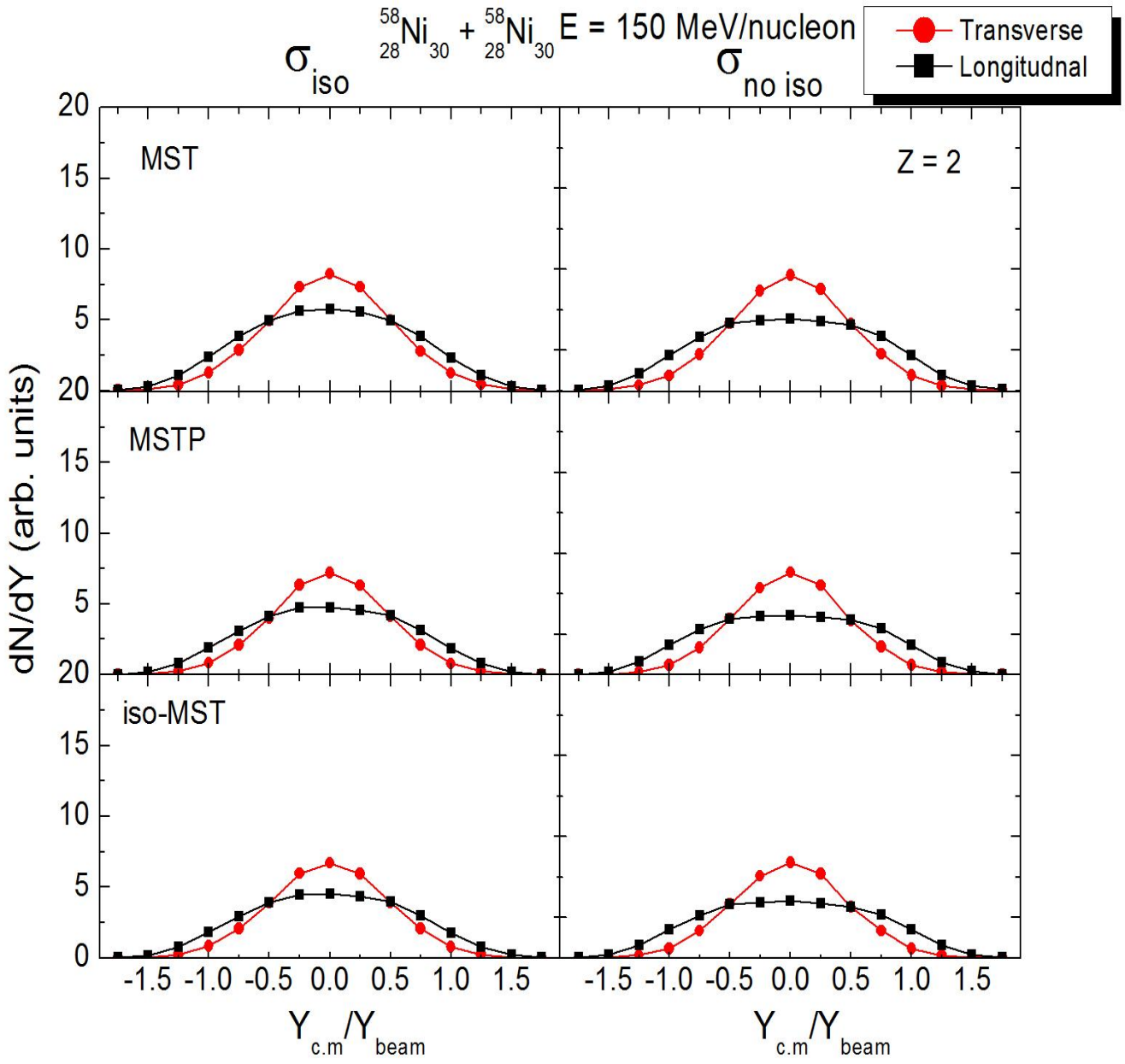

Fig. 3.4: Rapidity distribution as a function of $Y_{c.m}/Y_{beam}$ for $^{58}_{28}Ni$ + $^{58}_{28}Ni$ system at $\hat{b}$ = 0 fm and incident energy 150 MeV/nucleon, with σ_{iso} and $\sigma_{no\ iso}$

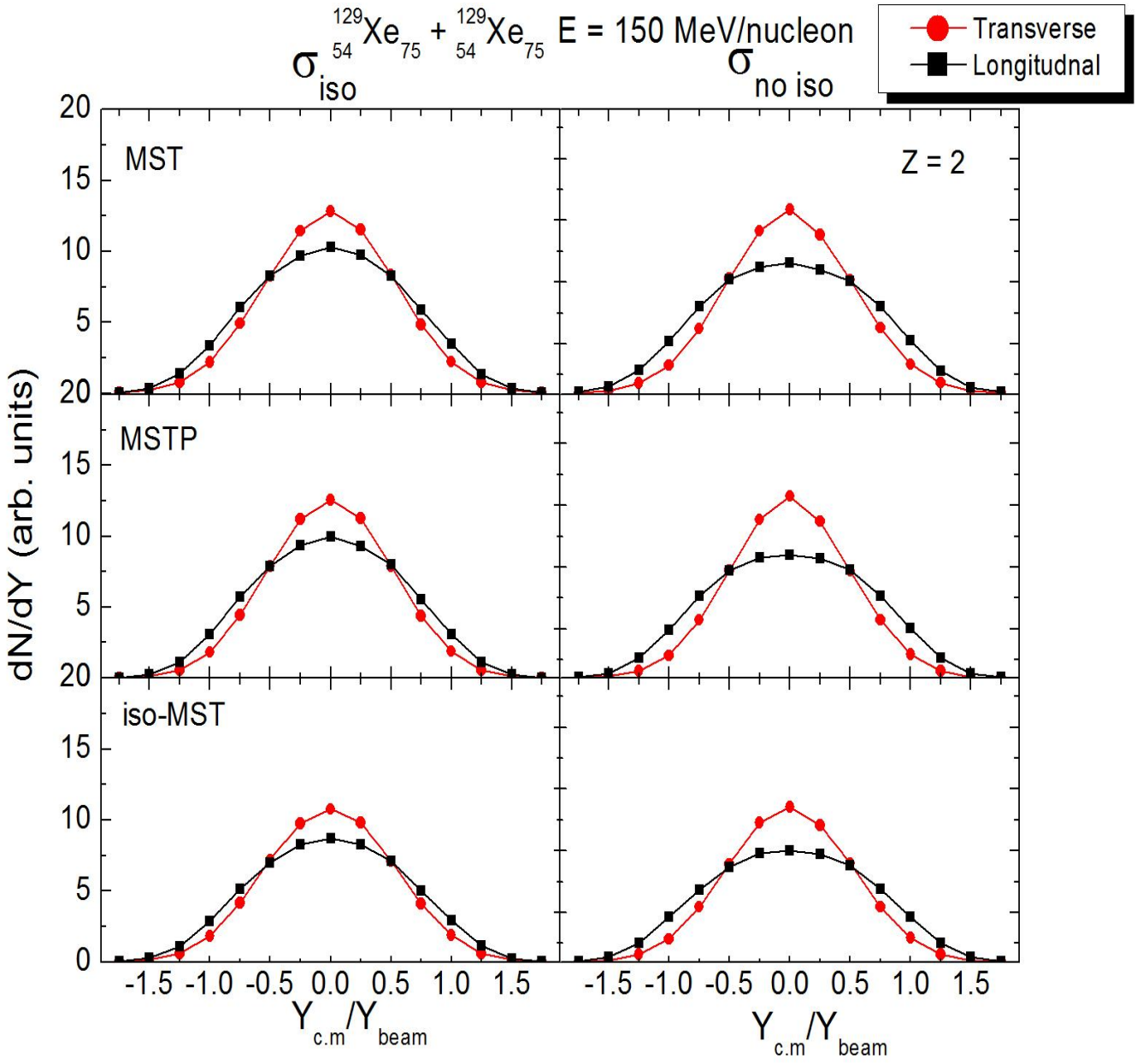

Fig. 3.5: Rapidity distribution as a function of $Y_{c.m}/Y_{beam}$ for $^{129}_{54}Xe$ + $^{129}_{54}Xe$ system at $\hat{b}$ = 0 fm and incident energy 150 MeV/nucleon, with σ_{iso} and $\sigma_{no\ iso}$

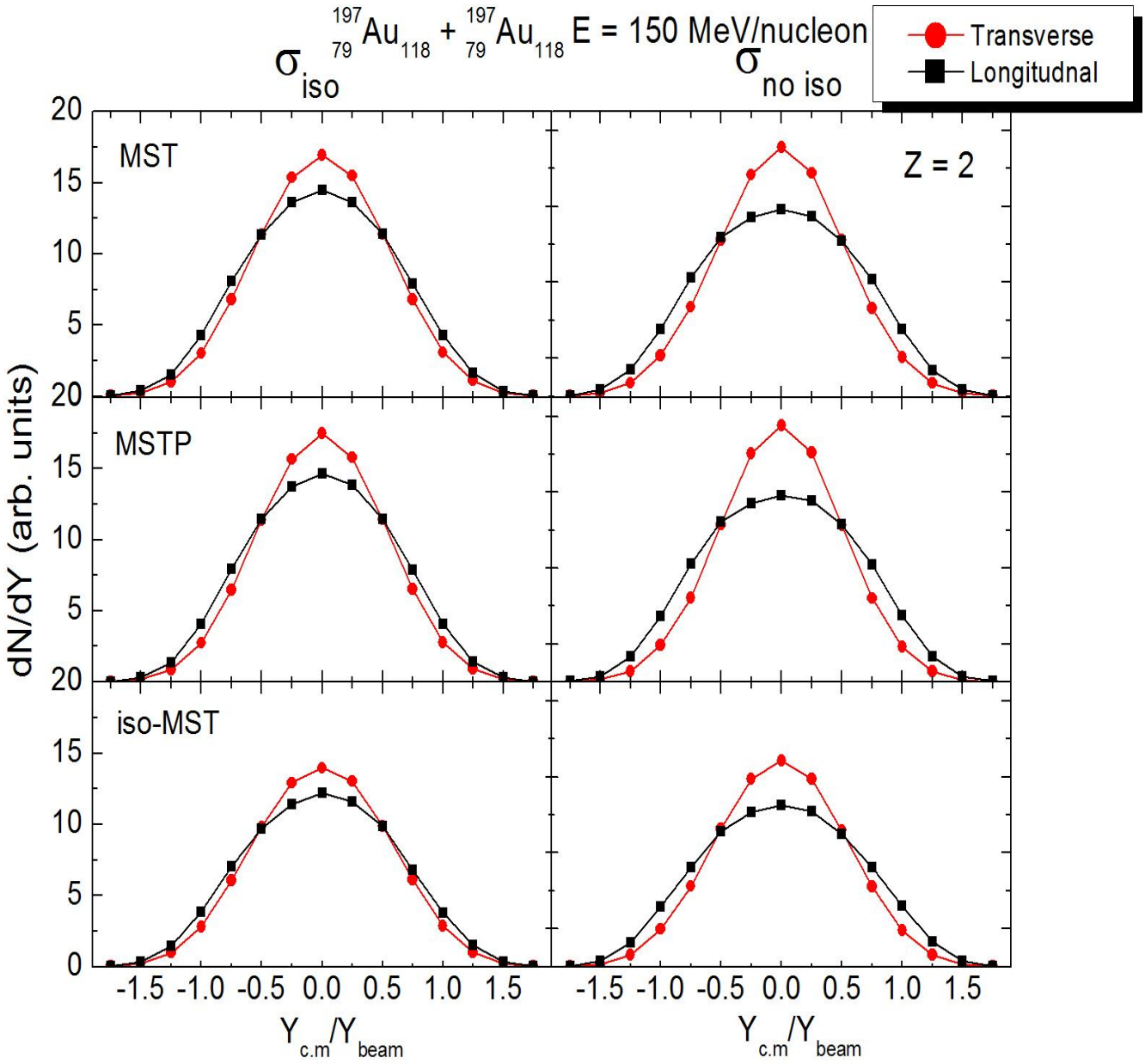

Fig. 3.6: Rapidity distribution as a function of $Y_{c.m}/Y_{beam}$ for $^{197}_{79}Au$ + $^{197}_{79}Au$ system at $\hat{b}$ = 0 fm and incident energy 150 MeV/nucleon, with σ_{iso} and $\sigma_{no\ iso}$

3.2.3 Variation of stopping parameter *varxz* with different clusterization algorithms

I. As a function of incident energy

In Fig. 3.7, we display *varxz* for protons as a function of incident energy for the system $^{197}_{79}$Au + $^{197}_{79}$Au at an impact parameter of $\hat{b} \leq 0.15$ and the same is done for fragment Z = 2 (Fig. 3.8) for the reactions of $^{40}_{20}$Ca +$^{40}_{20}$Ca, $^{58}_{28}$Ni +$^{58}_{28}$Ni, and $^{129}_{54}$Xe +$^{129}_{54}$Xe. The fine observations are:

1) The excitation function *varxz* is relatively low at lower energies (90-300 MeV/nucleon), rises to a maximum and then declines gradually. It is observed that *varxz* does not yield a value of 1 (corresponding to maximum stopping at central collisions) indicating that full thermalization is not achieved even for the heavier system in central collisions. The rising part of the *varxz* excitation function is due to the decreasing effect of pauli blocking and an increase in the repulsive mean field (due to increasing compression) with increasing energy in the range 150-400 MeV/nucleon. For heavier systems, i.e., $^{129}_{54}$Xe +$^{129}_{54}$Xe and $^{197}_{79}$Au +$^{197}_{79}$Au, a maximum of stopping is found at around 400 MeV/nucleon in agreement with the experimental data. This maximum reflects the combination of final state Pauli blocking and a decreasing cross-section. On the other hand, when energy exceeds 400-600 MeV/nucleon, a decline in the stopping excitation function, is seen. This is because, with increasing energy, the blocking becomes ineffective and the elementary cross-section drops resulting in less collisions and hence a lower stopping. For lighter systems, i.e. $^{40}_{20}$Ca +$^{40}_{20}$Ca and $^{58}_{28}$Ni +$^{58}_{28}$Ni, stopping is more at lower energies (at 90-150 MeV/nucleon), which gradually decreases and then follows the same trend as shown by the heavier systems.
2) The simulated points using different clusterization techniques (MST, MSTP, iso-MST) show slightly different values of *varxz*. The difference in influence of the three clusterization techniques is seen more in the lighter systems than in the heavier ones and at lower incident energies. One can observe that in general, *varxz* plot using MST algorithm shows a higher stopping as compared to the other clusterization techniques. This is because the iso-MST with larger values of R^{nn} and R^{np} will reduce the yield of nucleons and LCPs at mid-rapidity as more nucleons close to the cluster are absorbed into fragments. In other words, iso-MST reduces the multiplicities of nucleons and

low mass fragments and enhances the production of heavier fragments, hence, indicating lower stopping.

3) The theoretical magnitude of *varxz* shown by the $^{197}_{79}$Au + $^{197}_{79}$Ausystem is in disagreement with the experimental data although the trend shown by the excitation curve matches with that of the experiment. This difference in values is because of the various experimental filters that are imposed during the experiment.

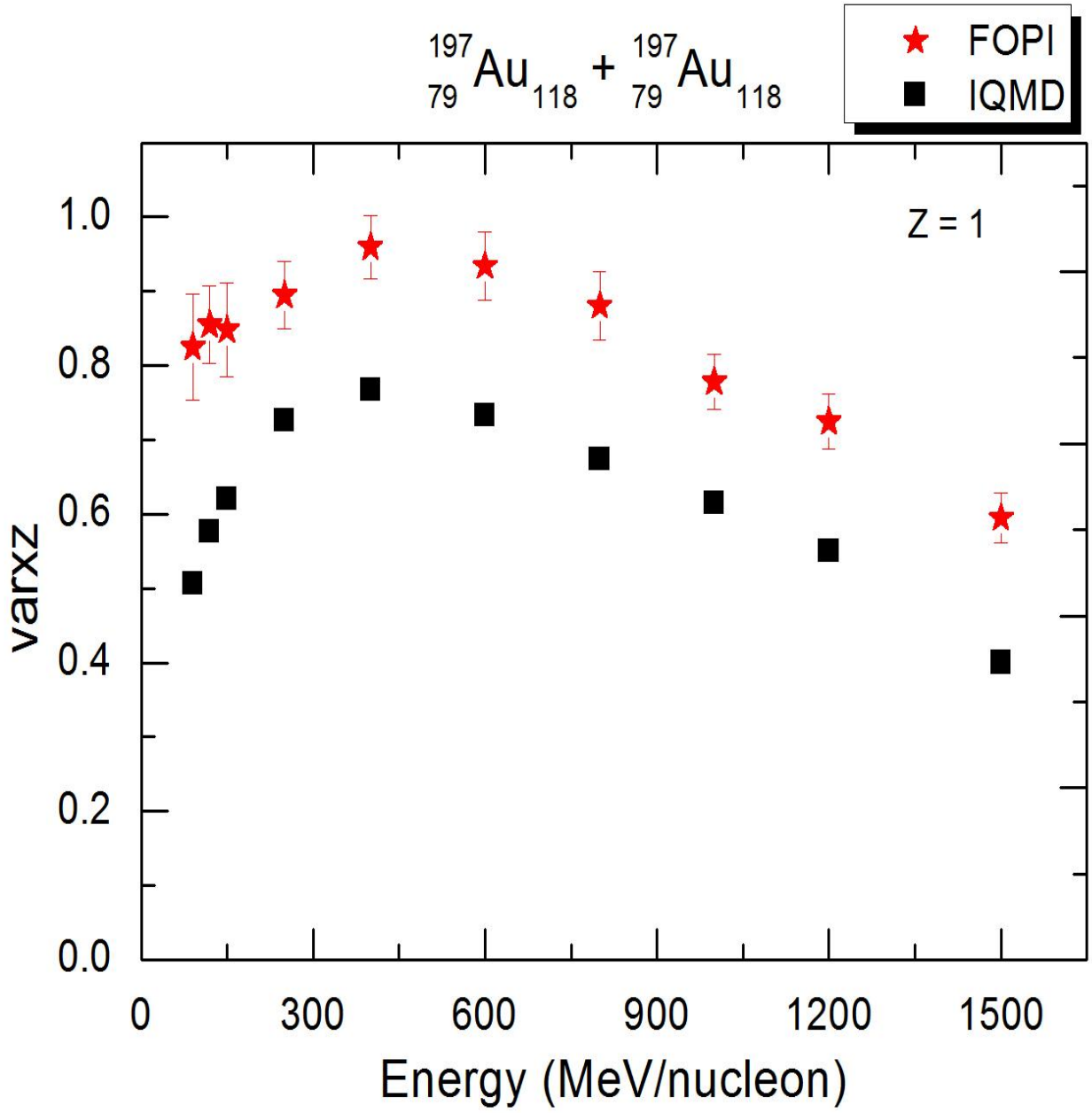

Fig. 3.7: *varxz* vs incident energy for protons for the system $^{197}_{79}$Au +$^{197}_{79}$Au with MST

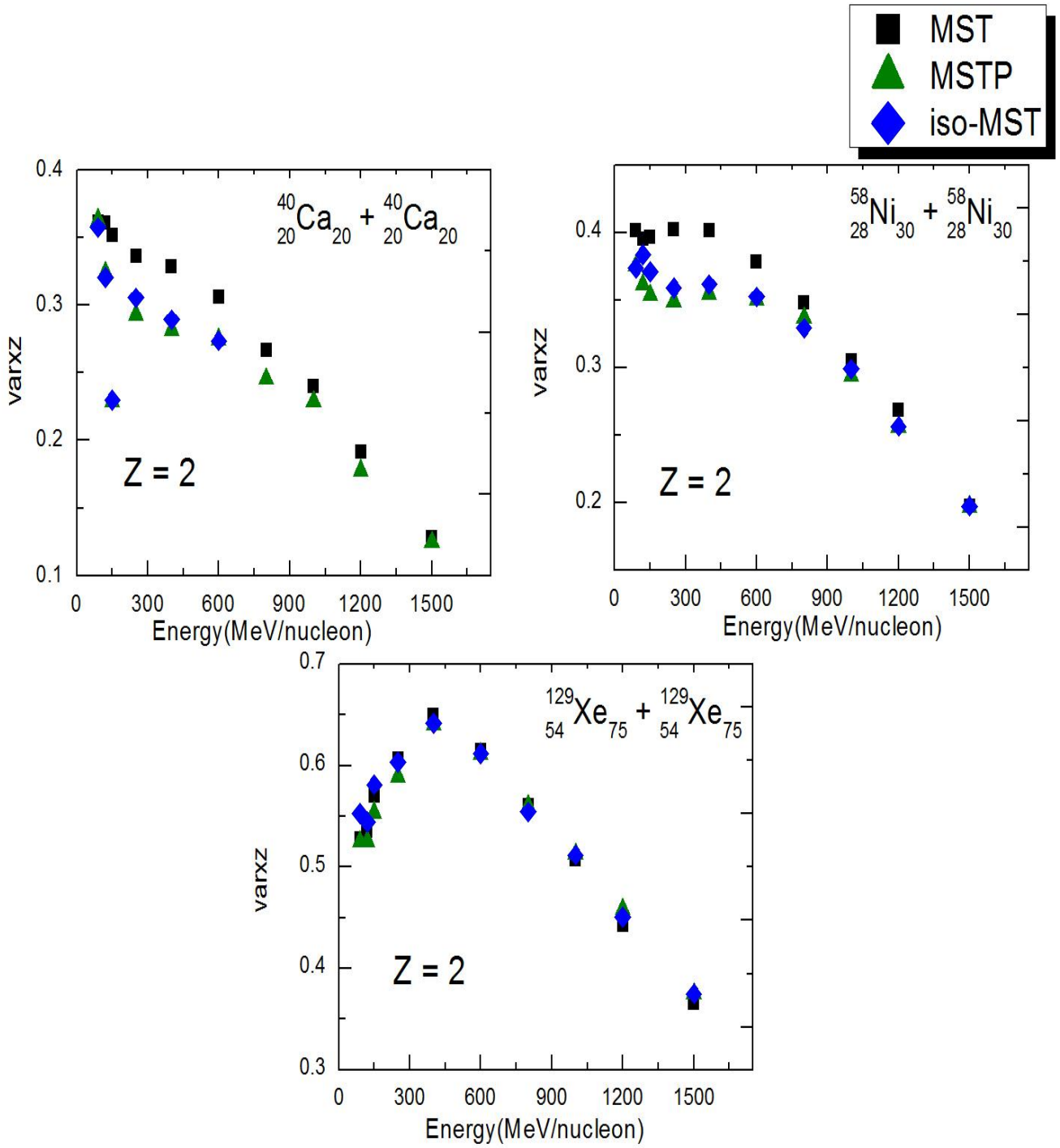

Fig. 3.8: *varxz* vs incident energy for fragment charge Z=2 with different clusterization algorithms

II. As a function of fragment charge (Z)

The influence of the different clusterization techniques on stopping variable varxz is now examined in Fig. 3.9 with various fragment charge (Z).

The trend shown by $^{58}_{28}$Ni +$^{58}_{28}$Ni and $^{197}_{79}$Au + $^{197}_{79}$Au systems follow the trend of the experimental data. It is observed that in general, *varxz* simulated using MST algorithm predicts a higher stopping than MSTP or iso-MST algorithms. Again, the reason is the same as discussed in the previous case. The difference is seen quite evidently for $^{40}_{20}$Ca +$^{40}_{20}$Ca (lighter) system. One can also conclude that in general, stopping decreases with increase in fragment charge (Z), being the maximum for Z=1. This is due to the fact that Z=1 corresponds to particles which originate from the participant region, where breaking of initial correlations among the nucleons is maximal and as a result, more randomization and stopping is achieved. The trends as observed in Fig. 3.9 suggest that the heavier fragments, even in rather central collisions, experience less stopping than lighter ones and keep a strong memory of the initial momentum.

III. As a function of scaled impact parameter ($\hat{b}$)

Fig. 3.10 shows the centrality dependence of stopping or influence of impact parameter $\hat{b}$ on *varxz* (of protons), for the reaction $^{197}_{79}$Au +$^{197}_{79}$Au. The same is done for reactions of $^{40}_{20}$Ca +$^{40}_{20}$Ca, $^{58}_{28}$Ni +$^{58}_{28}$Ni and $^{129}_{54}$Xe +$^{129}_{54}$Xe (Fig. 3.11) again investigated with the help of different clusterization algorithms. As expected, stopping is more for more central collisions and decreases with increasing $\hat{b}$ (in agreement with experiment). This is because, stopping is the phenomenon which originates from the participant zone and this zone goes on decreasing with increase in the impact parameter and hence the effect of cross-section on nuclear stopping decreases. One can again observe that MST clusterization yields a higher value of stopping at both central and peripheral collisions. The difference in *varxz* for simulations with different clusterization algorithms (MST, MSTP, and iso-MST) becomes more significant as impact parameter increases. And as mentioned earlier, the difference in the *varxz* plots using different clusterization algorithms reduces for higher incident energy (1500 MeV/nucleon). Again, this difference is more evident for lighter systems than in the heavier ones.

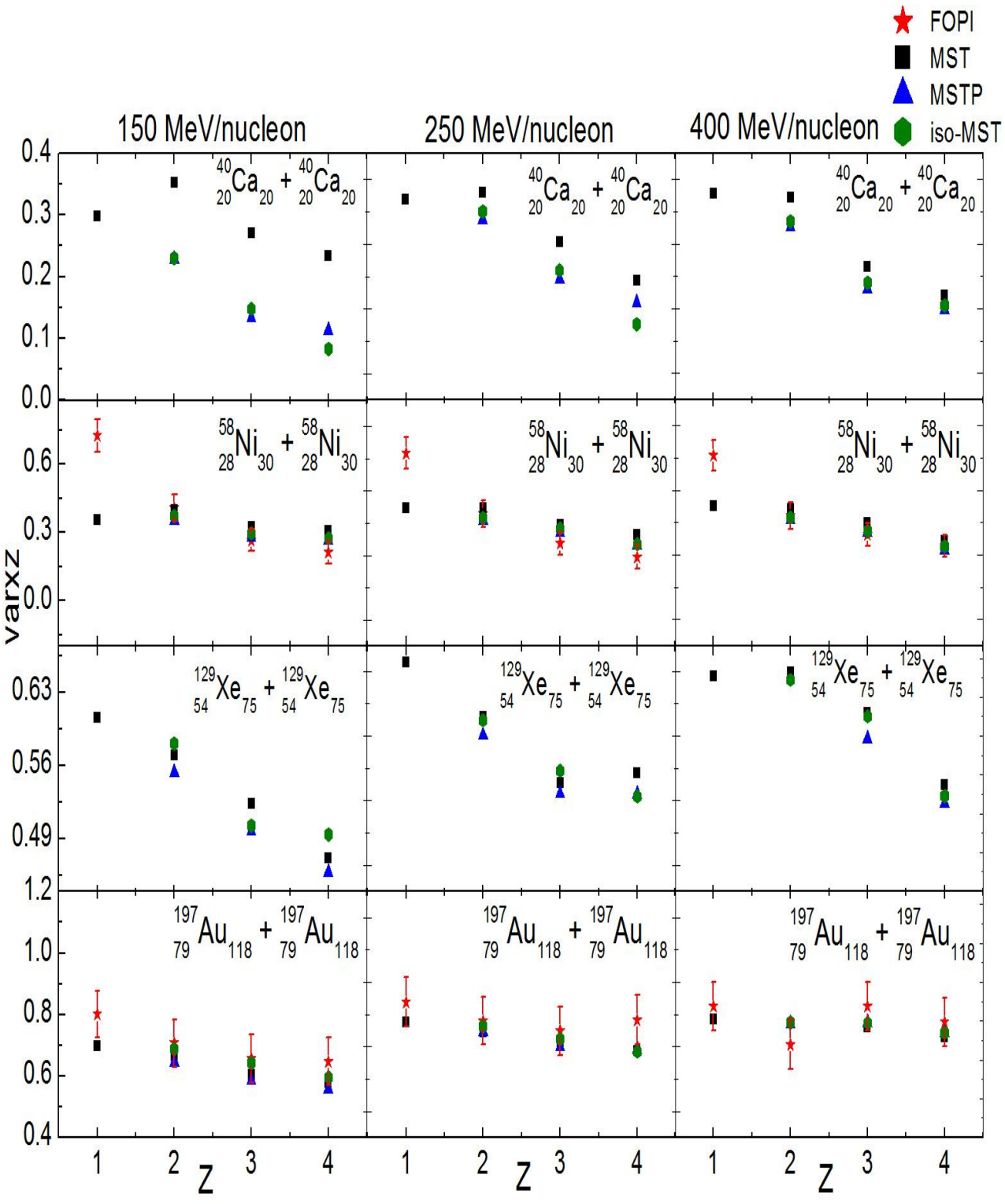

Fig. 3.9: *varxz* as a function of Z at incident energies 150, 250 and 400 MeV/nucleon with different clusterization algorithms.

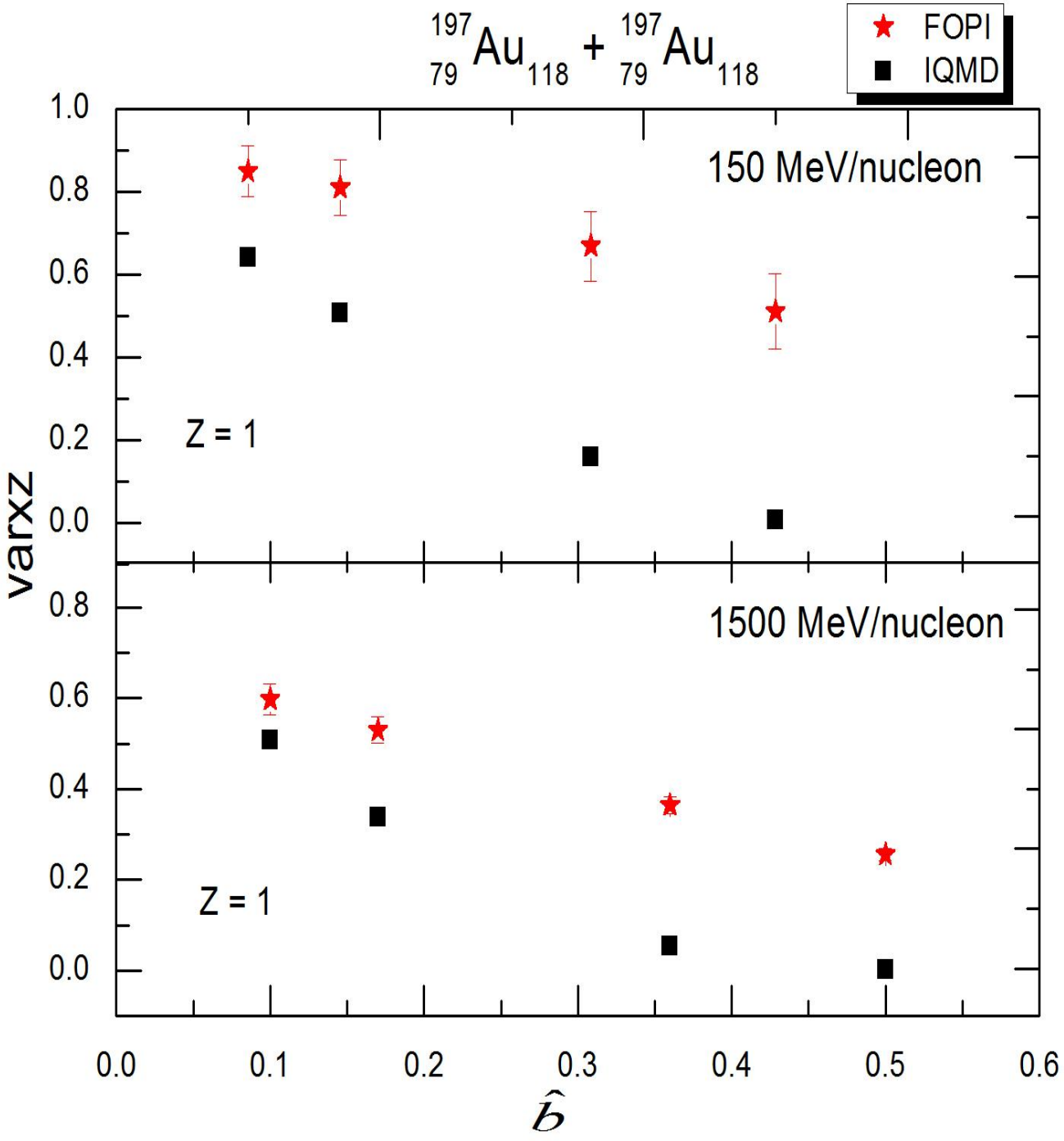

Fig. 3.10: *varxz* (of protons) vs $\hat{b}$ for $^{197}_{79}$Au +$^{197}_{79}$Au at incident energies 150 and 1500 MeV/nucleon with MST

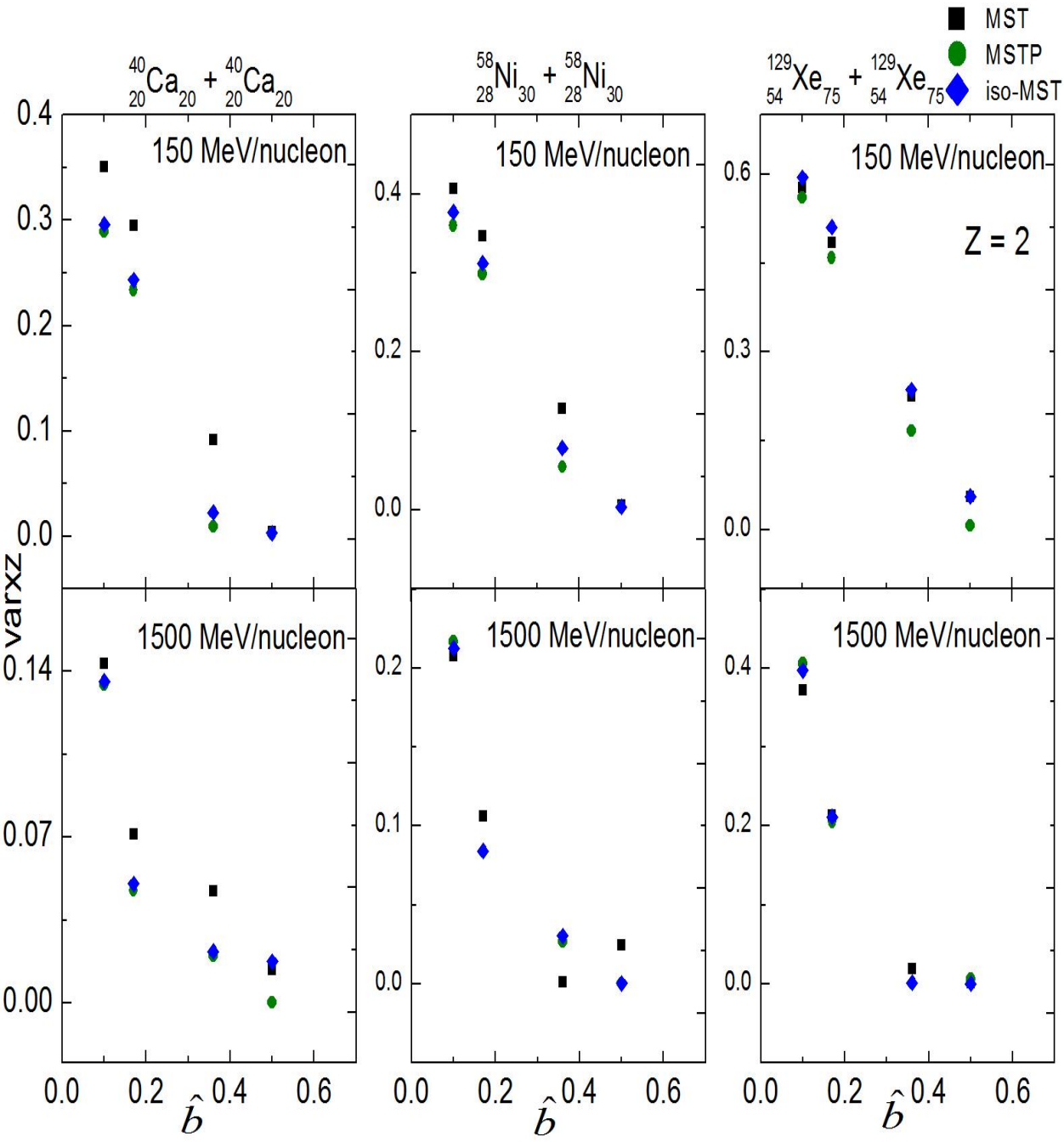

Fig. 3.11: *varxz* (of Z=2 fragment) vs $\hat{b}$ at incident energies 150 and 1500 MeV/nucleon with different clusterization algorithms.

3.2.4 Variation of stopping parameter *varxz* with isospin dependent (σ_{iso}) and isospin independent ($\sigma_{no\ iso}$) cross-section.

I. As a function of incident energy

Further, to study the influence of isospin dependence of nucleon-nucleon cross-section on nuclear stopping, we display in Fig. 3.12, the incident energy dependence of *varxz* for the similar systems as in the previous figures. It has been observed that isospin dependence of nucleon-nucleon cross-section plays a significant role at low incident energy (E < 400 MeV/nucleon). Moreover, the nuclear stopping is higher for σ_{iso} compared to $\sigma_{no\ iso}$. This happens because for isospin dependent cross-section, both singlet and triplet channels contribute, which enhances the nucleon-nucleon binary collisions. Therefore, the probability of collisions to take place increases, resulting in a higher stopping. In contrast, at higher incident energies, a violent phase of collisions takes place, and nuclear stopping becomes independent of isospin dependence of nucleon-nucleon cross-section.

II. As a function of system mass

To investigate the role of isospin dependence of the nucleon-nucleon cross section, Fig. 3.13 represents system size dependence of *varxz* at different energies=150, 250, 400, 1000, 1500 MeV/nucleon for fragment charge Z = 1,2,3,4 plotted using σ_{iso} and $\sigma_{no\ iso}$. From the graph, one can see the increasing trend of *varxz* with system mass for both σ_{iso} and $\sigma_{no\ iso}$. This is because higher density and temperature is reached in heavier systems than in the lighter ones, resulting in a higher degree of stopping. It is also observed that stopping in case of σ_{iso} is relatively more than with $\sigma_{no\ iso}$. This difference becomes less evident as incident energy increases, as explained previously.

In almost all cases, stopping for fragment charge Z=1 is more than the rest of the fragments which indicate that free nucleons experience more violent collisions, and hence experience more stopping. The difference in the *varxz* of various fragments becomes more prominent with increasing energy. For E=1000, 1500 MeV/nucleon, one can clearly see that *varxz* points for different fragments spread out indicating that different fragments experience different nuclear stopping at higher energies.

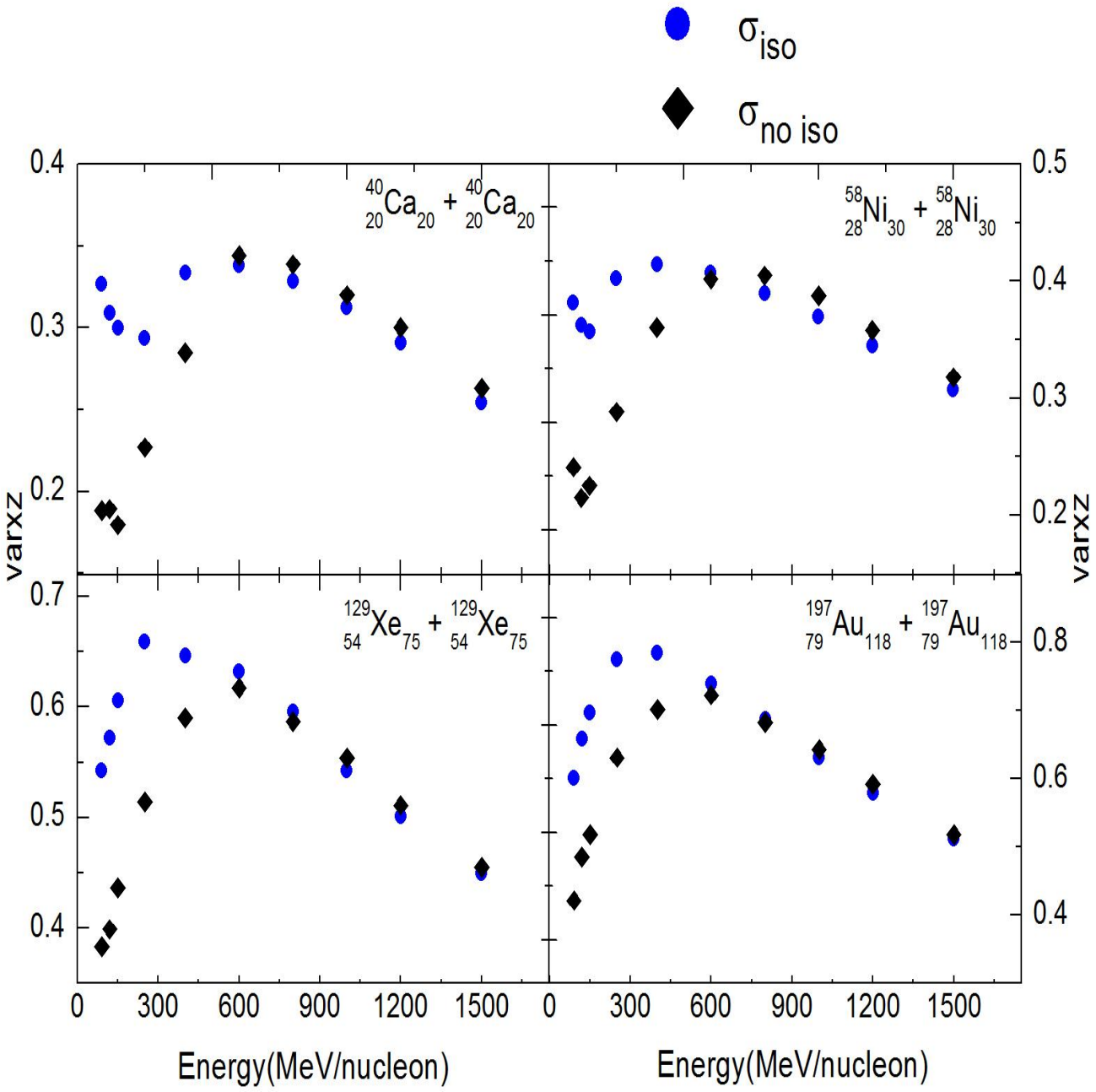

Fig. 3.12: *varxz* as a function of energy for σ_{iso} and $\sigma_{no\ iso}$ with MST

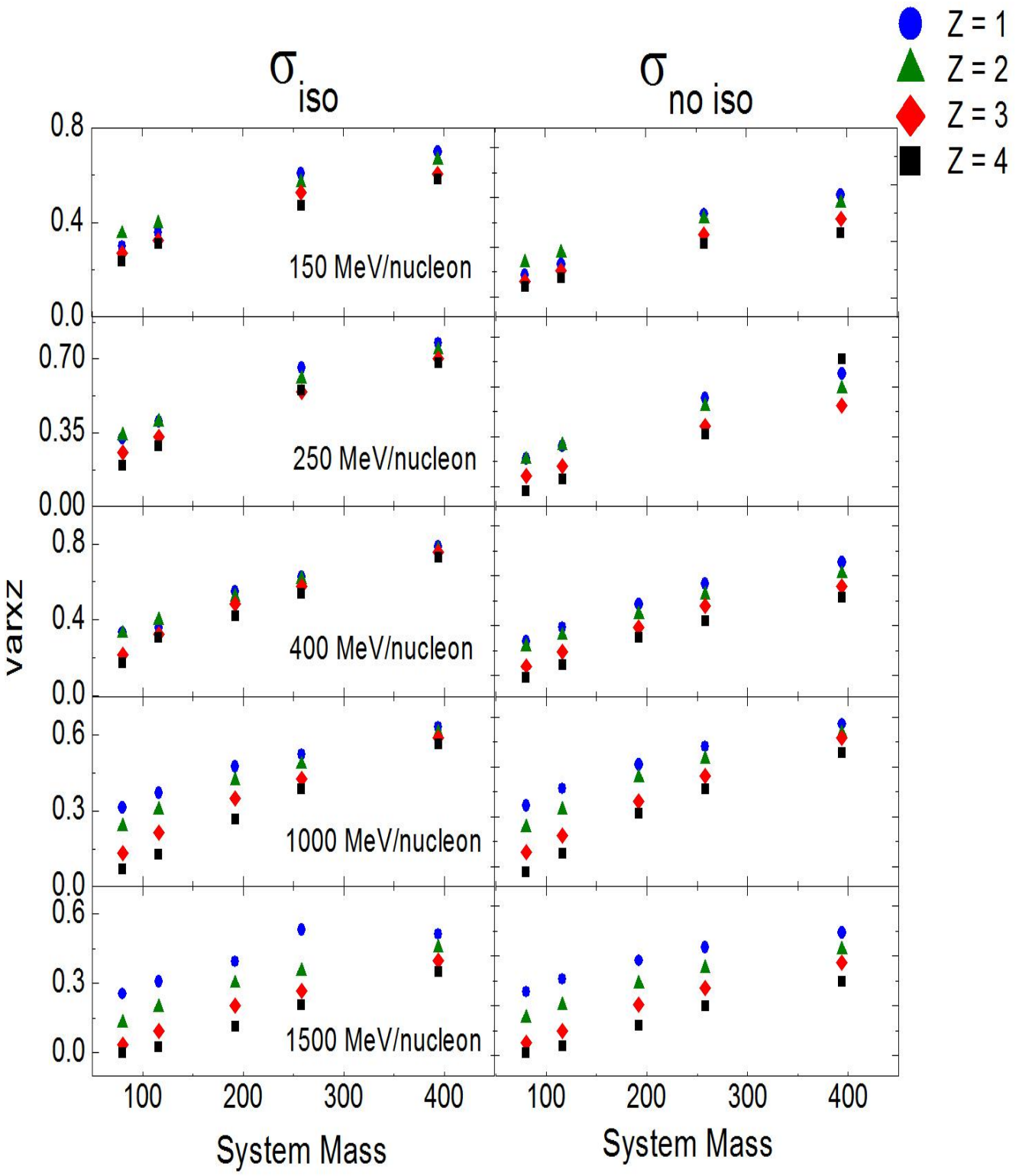

Fig. 3.13: *varxz* as a function of system mass for incident energies 150, 250, 400, 1000, 1500 MeV/nucleon using MST with σ_{iso} and $\sigma_{no\ iso}$

3.3 Conclusions

Using the Isospin Dependent Quantum Molecular Dynamics (IQMD) model, we have carried out simulations for the symmetric reactions $^{40}_{20}$Ca +$^{40}_{20}$Ca, $^{58}_{28}$Ni +$^{58}_{28}$Ni, $^{129}_{54}$Xe +$^{129}_{54}$Xe, and $^{197}_{79}$Au + $^{197}_{79}$Au in the energy range 90 MeV/nucleon – 1.5 GeV/nucleon. Stopping parameter *varxz* for protons and different fragment charge is calculated as a function of various parameters, taking into account both isospin dependent and isospin independent cross-section. We conclude that:

- A higher value of stopping is achieved in case of σ_{iso} than $\sigma_{no\ iso}$ at low incident energies (E < 400 MeV/nucleon). The influence of isospin dependence of the nucleon-nucleon cross-section decreases with increasing energy as well as impact parameter.
- Thermalization and stopping achieved in heavier systems is greater as compared to the lighter ones. The isospin effects of cross-section do not play any significant role in the rapidity distribution.
- The excitation function *varxz* for protons is initially low at lower incident energies (90-300 MeV/nucleon), rises to a maximum and then declines gradually in agreement with experimental data. It is observed that *varxz* does not yield a value of 1, indicating that full thermalization is not achieved even for the heavier systems in central collisions.
- *varxz* plot for fragments using MST algorithm shows a higher stopping as compared to other clusterization techniques. This difference is seen more for lighter systems than the heavier ones and at lower incident energies.
- Stopping decreases with increase in fragment charge (Z), being the maximum for Z=1.
- The degree of stopping is more for more central collisions and decreases with increasing $\hat{b}$ following the same trend of experimental data. The difference in *varxz* for simulations with different clusterization algorithms (MST, MSTP, and iso-MST) becomes more significant as impact parameter increases.
- It is observed that *varxz* increases with system mass. It is also noted that the difference in the *varxz* of various fragments becomes more prominent with increasing energy.

References

[1] W. Scheid, R. Ligensa, and W. Greiner, Phys. Rev. Lett. **21**, 1479 (1968)

[2] L. P. Csernai and J. I. Kapusta, Phys. Rep. **131**, 225 (1986)

[3] R. Stock, Phys. Rep. **135**, 261 (1986)

[4] H. Stocker and W. Greiner, Phys. Rep. **137**, 277 (1986)

[5] R. B. Clare and D. Strottman, Phys. Rep. **141**, 179 (1986)

[6] B. Schurmann, W. Zwermann and R. Malfiet, Phys. Rep. **147**, 3 (1986)

[7] W. Cassing, V. Metag, U. Mosel and K. Niita, Phys. Rep. **188**, 361 (1990)

[8] J. Aichelin, Phys. Rep. **202**, 233 (1991)

[9] S. Kumar, Ph.D, Thesis, P.U. Chandigarh (2000)

[10] L.C.Vaz, J. M. Alexander and G. R. Satchler, Phys. Rep. **69,** 373 (1981); M. Beckerman, Rep. Prog. Phys. **51**, 1047 (1988). K. E. Zyromski, *et al*., Phys. Rev. C **55**, R562 (1997).

[11] H. Ngo and C.H. Ngo, Nucl. Phys. A **348**, 140 (1980); K. C. Panda and T. Patra, J. Phys. G **14**, 1489 (1988).

[12] R. K. Puri, Ph.D. Thesis, P.U. Chandigarh, (1990)

[13] M. K. Sharma, Ph.D. Thesis, P.U. Chandigarh, (1998)

[14] S. Kumar, Ph.D, Thesis, Thapar University, Patiala (2010)

[15] H. Stocker and W. Greiner, Phys. Rep. **137**, 277 (1986)

[16] G. Q Zhang, Y. G Ma, *et al.*, Phys. Rev. C **84**, 034612 (2011)

[17] Q. Li and Z. Li, Chin. Phys. Lett. **19**, 321 (2002).

[18] J. Y. Liu, W. J. Guo, S. J. Wang, W. Zuo, Q. Zhao, and Y. F. Yang, Phys. Rev. Lett. **86**, 975 (2001).

[19] S. Kumar, S. Kumar, R. K Puri, Phys. Rev. C **81**, 014601(2010)

[20] C. Hartnack, *et al*., Eur. Phys. J. A **1**, 167(1998)

[21] J. Singh, S. Kumar, and R. K. Puri, Phys. Rev. C **62**, 044617 (2000); *ibid*. **65**, 024602 (2002); R.K. Puri and S. Kumar, ibid. **57**, 2744 (1998); S. Kumar and R. K. Puri, *ibid*. **58**, 2858 (1998); S. Kumar, S. Kumar, R. K. Puri, *ibid*. **78**, 064602 (2008); S. Kumar, S. Kumar, and R. K. Puri, Phys. Rev. C **81**, 014601 (2010).

[22] S. Kumar and R. K. Puri, Phys. Rev. C **57**, 320 (1998); J. Singh and R. K. Puri, *ibid*. **62**, 054602 (2000).

[23] Y. Zhang, Z. Li, *et al.*, Phys. Rev. C **85**, 051602 (2012)

[24] L. G. Moretto, D. N. Delis, and G. J. Wozniak, Phys. Rev. Lett. **71**, 3935 (1993).

[25] L. Phair *et al*., Phys. Rev. Lett. **75**, 213 (1995); L. Phair et al., Phys. Rev. Lett. **77**, 822 (1996).

[26] Y. Zhang *et al*., Phys. Lett. B **664**, 145 (2008).

[27] M. B. Tsang *et al*., Phys. Rev. C **76**, 041302 (R) (2007); M. Mocko *et al*., Eur. Phys. Lett. **79**, 12001 (2007).

[28] T. X. Liu *et al*., Phys. Rev. C **76**, 034603 (2007).

[29] G. Lehaut, D. Durand, *et al.*, PRL **104**, 232701 (2010)

[30] W. Reisdorf, *et al.*, Nucl. Phys. A **848** (2010) 366–427

[31] S. Piantelli *et al*., Phys. Rev. C **74**, 034609 (2006); S. Piantelli *et al*., Phys. Rev. C **78**, 064605 (2008).

[32] D. V. Shetty *et al*., Phys. Rev. C **68**, 054605 (2003); D. V. Shetty, S. J. Yennello and G. A. Souliotis, Phys. Rev. C **75**, 034602 (2007).

[33] A. K. Kerman and S.E. Koonin, Ann. of Phys. **100,** 332 (1976)

[34] J. Cugnon, T. Mizutani and J. Vandermeulen, Nucl. Phys. A **352**, 505 (1981)

[35] G.F. Bertsch, H. Kruse and S. Das Gupta. Phys. Rev. C **29**, R673 (1984)

[36] J. Aichelin and G. Bertsch. Phys. Rev. C **31**, 1730 (1985)

[37] W. Bauer, D. Westfall, *Advances in Nuclear Dynamics 2* (Springer Publication, 1996)

.